CAPTURE OF GASEOUS SULFUR DIOXIDE USING GRAPHENE OXIDE BASED COMPOSITES

Tanushree Sankar Sanyal

Thesis submitted to the

Faculty of Engineering

In partial fulfillment of the requirements for the degree of

MASTER OF APPLIED SCIENCE in

Chemical Engineering

Department of Chemical and Biological Engineering

Faculty of Engineering

University of Ottawa

February 2021

Abstract

Sulfur dioxide (SO_2), a well-known pollutant emitted from fossil fuel combustion, has major adverse health and environmental impacts. It is harmful at low concentration with a permissible exposure limit of two ppm for the eight-hour time-weighted average (TWA) value. Fortunately, its atmospheric concentration, like other air pollutants, has gradually reduced in Canada in the past years. However, despite the well-established flue gas desulfurization technologies, they have the disadvantages of being energy-intensive, not very efficient to achieve very low concentrations (at ppm level) and they operate at high temperatures. Moreover, emission standards are becoming more stringent.

Novel methods are therefore investigated to capture SO_2, such as adsorption processes using zeolites and metal oxides (e.g., Iron (Fe) and Vanadium (V) based) which tend to sustain wide ranges of temperatures and pressures. Graphene oxide (GO) was also shown to physisorb SO_2 at low temperatures. In this work, we propose to metal functionalize GO as a step forward on the path for efficient SO_2 capture, by promoting the SO_2 oxidation reaction into sulfur trioxide (SO_3) for increased capacity due to a possible higher affinity with the surface. The GO has a high surface area, high porosity, and controllable surface chemistry. The aim is to achieve outlet concentration of SO_2 as low as 1 ppm through combined physisorption and reaction promoted that the presence of GO and metal, at low operating temperature.

Iron oxide functionalized GO was synthesized using two different techniques: a polyol process (GO-Fe_xO_y-P) and using a hydrolysis method (GO-Fe_xO_y-H). The characterization analysis, scanning electron microscopy (SEM) and transmission electron microscopy (TEM), performed on the materials before and after SO_2 reaction show changes on the surface due to metal adding and

to the sulfur capture. The breakthrough curves and the capacity calculations of the performed experiments have shown that with the addition of Fe_xO_y on the surface of GO, the capturing capacity increases by a factor of three to four, indicating a possible change in the capturing mechanism. The evaluation of the temperature effect (from room temperature to 100°C) showed an increasing trend in the capture capacity for SO_2 with an increase in temperature, for both functionalized and non-functionalized GO, indicating it is not driven only by surface adsorption. The presence of sulfur species captured from the gas stream has been confirmed by energy-dispersive X-ray (EDXS) analysis. The future work would be focused on the investigation of the mechanisms and capturing phenomenon and the regeneration step for the materials in order to further improve the capturing capacity and process applicability.

Résumé

Le dioxyde de soufre (SO_2), un polluant bien connu émis par la combustion de carburants fossiles, a des effets néfastes majeurs sur la santé et l'environnement. Il est nocif à faible concentration avec une limite d'exposition maximale de deux ppm pour la valeur moyenne pondérée dans le temps (TWA) sur huit heures. Heureusement, sa concentration atmosphérique, comme d'autres polluants atmosphériques, a progressivement diminué au Canada au cours des dernières années. Cependant, bien que des technologies soient bien établies pour la désulfuration gaz émis, ces procédés ont les inconvénients d'être énergivores et de fonctionner à haute température ainsi que d'être peu efficaces pour atteindre de très faibles concentrations (au niveau ppm). De plus, les normes d'émission deviennent maintenant de plus en plus strictes.

De nouvelles méthodes sont donc étudiées pour capturer le SO_2, tels que des procédés d'adsorption utilisant des zéolites et des oxydes métalliques (par exemple à base de fer (Fe) ou de vanadium (V)) qui peuvent supporter de grande variation de température et de pression. Il a également été démontré que l'oxyde de graphène (*GO*) pouvait physisorber le SO_2 à basse température. Dans ce travail, nous proposons de fonctionnaliser du GO avec du métal, afin de favoriser la réaction d'oxydation du SO_2 en trioxyde de soufre (SO_3) pour améliorer la capacité, puisque ce dernier peut avoir une plus grande affinité avec la surface. Le GO a une surface spécifique élevée, une porosité élevée et une chimie de surface contrôlable. L'objectif est d'atteindre une concentration de sortie de SO_2 aussi faible que 1 ppm grâce à une physisorption et une réaction combinées favorisées par la présence de métal sur le GO, à basse température de fonctionnement.

Le GO fonctionnalisé à l'oxyde de fer a été synthétisé à l'aide de deux techniques différentes: un procédé polyol (GO-Fe_xO_y-P) et une méthode d'hydrolyse (GO-Fe_xO_y-H). La caractérisation, par microscopie électronique à balayage (*SEM*) et par microscopie électronique à transmission (*TEM*), réalisée sur les matériaux avant et après la réaction SO_2 a montrée des changements en sur la surface à la suite de l'ajout de métal et à la capture du soufre. Les courbes de percée et les calculs de capacité des expériences réalisées ont montré qu'avec l'ajout de Fe_xO_y à la surface de GO, la capacité de capture augmente d'un facteur trois à quatre, indiquant un changement possible du mécanisme de capture. L'évaluation de l'effet de la température (de la température ambiante à 100 °C) a montré une tendance à la hausse de la capacité de capture du SO_2 avec une augmentation de la température, aussi bien pour les GO fonctionnalisés que non fonctionnalisés, indiquant qu'il n'y a possiblement pas que de l'adsorption en surface. La présence de soufre capturé du gaz a été confirmée par spectroscopie de rayons X à dispersion d'énergie (*EDXS*). Les travaux futurs porteront sur l'étude des mécanismes du phénomène de capture et sur l'étape de régénération des matériaux afin de continuer à améliorer la capacité de capture et l'applicabilité du procédé.

Acknowledgments

First and foremost, I would like to express my deepest gratitude to Professor Clémence Fauteux-Lefebvre and Professor Andrew Sowinski for taking me under their wing and guiding me throughout this project. The project would have not been successful without their continuous motivation, discussions, and their time, effort, and support.

I also wish to thank Professor Elena Baranova and her student Christopher Panaritis for introducing a new method of synthesis of graphene oxide – iron oxide nanoparticles composite and providing inputs throughout the process.

I would also like to thank the support staff Franco Ziroldo, Gérard Nina, and James Macdermid – for their technical and mechanical support in building the experimental setup. I would also like to thank the administrative staff Francine Petrin, Frantz Célestin, Sylvie Saindon, and Chantal Dube. I would like to thank Dr. Yun Liu for helping us out with the TEM and EDXS analysis along with David Diekrup and Renelle Dubosq for assisting us with the SEM analysis.

A hearty thanks to my lab mates, Saleh Bischara Sennousi and Raheleh Zafari, for their assistance throughout the project.

I would also like to express my gratitude to Dr. C.K. Modi and Dr. Ravi S. Vithalani, from M.S. University Baroda, for introducing me to graphene oxide

I would also like to appreciate the support and care of my friends both from back at home, India, and the new family of friends I made here.

At last, I would like to thank Natural Sciences and Engineering Research Council (NSERC) and uOttawa for funding our research work.

I would like to express my indebtedness towards my parents by dedicating my thesis work to them,

Dr. Sankar P. Sanyal and Mrs. Chandana Sanyal.

Table of Contents

List of Figures

List of Tables

Nomenclature and Abbreviations

Å	Armstrong
AC	Activated Carbon
AQA	Air Quality Agreement
AQC	Air Quality Committee
CCME	Canadian Council of Ministers of the Environment
CEPA	Canadian Environmental Protection Act
DFT	Density Functional Theory
EDXS	Energy Dispersive X-ray Spectroscopy
FGD	Flue Gas Desulfurization
GO	Graphene Oxide
HRTEM	High-Resolution Transmission Electron Microscopy
MERAF	Multi-pollutant Emission Reduction Analysis Foundation
MO	Metal Oxides
MOFs	Metal-Organic Frameworks
NO_x	Nitrogen Oxides
PAN	Polyacrylonitrile
PM	Particulate Matter
ppm	Parts per million
SEM	Scanning Electron Microscopy
SO_2	Sulfur Dioxide
SO_x	Sulfur Oxides

TEM	Transmission Electron Microscopy
TRS	Total Reduced Sulfur
TWA	Total Weighted Average
UNECE LRTAP	United Nations Economic Commission for Europe Convention on Long-Range Transboundary Air Pollution
VOC	Volatile Organic Compound
XPS	X-ray Photoelectron Spectroscopy

Co-Authorship Statement and Thesis Content

I declare that I am the first author of all the chapters written in this thesis.

I acknowledge the supervision of Prof. Clémence Fauteux-Lefebvre and Prof. Andrew Sowinski on the work described in this thesis, their editorial comments on the written document, and their scientific guidance in preparing and performing laboratory experiments as well as analyzing the results.

Chapter 1 is the introduction to the thesis work and a brief description of the problems, thesis objectives, and an overview of the thesis.

Chapter 2 presents the literature review which provides a detailed insight into the problem and the steps taken to mitigate sulfur dioxide. It moves forward with an introduction to the solution suggested in this thesis work, functionalization, and applications.

Chapter 3 details the methodology applied to achieve the thesis objectives.

Chapter 4 describes the results obtained after experiments and characterizations and their analysis. Chapters 2, 3, and 4 will be combined to be submitted as an article in a scientific journal.

Chapter 5 concludes the thesis work and provides some prospective future work.

CHAPTER 1
INTRODUCTION

Air pollution has played a major role in decaying the environment of Earth. Due to the release of harmful toxic chemicals into the atmosphere, the air quality has been deteriorating rapidly [1]. This is in addition to the global increase in greenhouse gas emissions causing global warming, with one of the most recent tangible or visual effects has been seen in the breaking of the largest floating block of ice in Antarctica, A-68 [2]. With the intensification of global warming along with urbanization and industrialization, stricter rules and regulations need to come into play to reduce the negative impacts of pollutant emissions considerably and rapidly.

The major toxic gases emitted from industries mainly consist of particulate matter, nitrogen, sulfur, and carbon oxides. Amongst all these pollutants emitted from the flue gas stream approximately 87% SO_x and 67% NO_x are emitted from the fossil fuel-fired plants [3]. These acidic gases have been considered as the most toxic and harmful gases and are believed to contribute to the increasingly serious environmental conditions by causing problems like an increase in the acidity of water bodies through acid rain.

SO_2, a colourless and odorless gas, has a Time Weighted Average (TWA) of 2 ppm for 8 hours, thus even a low concentration of 2 ppm is harmful to humans. Respiratory problems like asthma on a single exposure to a high SO_2 concentrated area, shortness of breath, coughing, on inhalation; skin burns, blistering and permanent scarring when the skin is exposed to SO_2; and burning of eyes when SO_2 comes in contact with the eyes, are a few effects of the acidic gas on humans [4]. The impact of SO_2 on the environment is mainly through acid rain, photochemical smog, and ozone

layer depletion [3]. These in turn damage the vegetation and affect the wildlife along with an increase in the acidity of water bodies.

The major emission of SO_2 is from the power plants which use fossil fuels as the main source of power. The dependency of the energy sector on fossil fuels has gradually decreased but it still ranks amongst the top sources of fuel. This can be due to the inflation of prices of other fuel sources, and in the next twenty years, coal will be one of the significant fuels for power generation across the world [3].

Decades of efforts have been made to reduce the SO_2 emissions by introducing stringent rules for air quality control from the industries, shifting towards low sulfur content fuels, and removal of sulfur from coal before combustion [5]. There has been remarkable progress made by developed countries, but the setback is faced from the still-developing countries, because of the growth in electricity demand and absence of proper regulations for SO_2 control [6].

To reduce SO_2 emissions in Canada, more stringent rules have been adopted across the world. In Canada, four provinces – New Brunswick, Nova Scotia, Quebec, and Ontario, have complied with specific regulations and the Canada-wide Acid Rain Strategy [7].

1.1 How to capture SO_2?

Despite the variety of technologies existing to decrease SO_2 production and emission levels, there is an urgent need for new efficient removal technologies for these contaminants. They must be applicable at low temperature (target of 100°C maximum) to build energy-efficient processes that have a low concentration of residual contaminants in the outlet gas, i.e., a target of 1 ppm, to meet stringent regulations. Regarding temperature, the lowest operation limit for removal of SO_2 is currently around 500°C [8], leading to energy-intensive or inefficient processes [9].

Flue gas desulfurization (FGD) units are established to reduce the emission of SO_2 in the flue gases and the wet FGD plants have been 92% -97% efficient in the removal of SO_2. But due to the high corrosive environment, high consumption of energy and water along with huge operational and maintenance costs have limited its use in small industrial plants [6,10]. Low-temperature processes to increase energy efficiency and lower achieved outlet concentrations to comply with new regulations are then needed.

Adsorptive materials like zeolites, metal, metal oxides and metal-organic frameworks provide alternatives for FGD. Zeolites, which are commonly also used in filtration and catalysis, can capture SO_2 in its microporous framework. Metals (iron, vanadium, copper) provide active sites for SO_2 adsorption and subsequent oxidation to SO_3. Even though metal oxides can capture SO_2, only a few can convert it to SO_3 [11,12].

1.2 Graphene oxide, a suitable multifunctional material

Graphene oxide (GO), a 2-dimensional crystal structure of sp^2 hybridised carbon, posses oxygenated functional groups such as hydroxyl and epoxy groups decorated on the surface and the carboxylic groups on the edges. The hydrogen bonding provides a hydrophilic nature in turn making it a high dispersive material in water or other polar solvents [13]. GO can be easily synthesized by Modified Hummer's Methods in small quantities [14]. The applications of GO are spread across various fields – electronics, electrical, chemical. Researchers have used GO for the removal of heavy metals, dyes, anti-biotic wastes, and for the removal of nitro-aromatics [15,16].

Graphene oxide provides sites for SO_2 adsorption and subsequent oxidation with the help of oxygen functionalities present on the surface. In this project, we are functionalizing GO with Iron (Fe) and Iron oxide nanoparticles to use them as capturing multifunctional materials.

1.3 Thesis objectives

The general objective of this thesis research project is to capture SO_2 at low temperatures using iron functionalized graphene oxide-based materials to obtain a very low concentration effluent. The research hypothesis is that the functionalization of GO with iron nanoparticles will enhance its capturing capacity by promoting a gas-solid reaction from SO_2 to SO_3, in addition to the adsorption.

The specific objectives were to:

1. Functionalize GO with iron oxide nanoparticles using a polyol method.
2. Functionalize GO with iron oxide nanoparticles using a hydrolysis method.
3. Achieve a low outlet concentration of a maximum of 1 ppm from a 35 ppm gas in a flow system, at temperatures below 100 °C.
4. Compare and characterize the various synthesized materials to get an understanding of the capturing mechanisms.

1.4 Thesis structure

This thesis is divided into 5 chapters. **Chapter 2** presents the Literature Review covering the methods and materials used to reduce SO_2 concentration followed by the introduction of GO and its properties and GO functionalization. **Chapter 3** details the methodology related to the thesis's objectives. **Chapter 4** presents results obtained after characterization, comparison, and their analysis. **Chapter 5** concludes with prospective future works.

CHAPTER 2
COMPREHENSIVE LITERATURE REVIEW

2.1 Sulfur Dioxide

The presence of SO_2 in the atmosphere has always been one of the main reasons for degrading the respiratory conditions for humans along with increasing the toxicity of the environment. Difficulties in breathing, intensifying cardiovascular diseases to a fatal level and respiratory illness are key health concerns linked with prolonged exposure to SO_2 [17]. Inhalation of SO_2 at a low concentration for a short time as 10 mins can constrict bronchi and induce throat inflammation [18].

The presence of acidic gas in natural environments has caused acidification of the water bodies as well as damage to vegetation and crops. The high acid deposition has stepped up the process of decay of the buildings and monuments [19]. The oxidizing radicals like O_3 and OH^- can convert SO_2 into aerosol particles of sulfuric acid which when mixed with rain will lead to the formation of acid rain and such causing acidifying pollution [20]. Moreover, the sulfate aerosols present in the clouds can reflect sunlight into space, making clouds more reflective and causing a net cooling in turn disturbing the climate and causing climate perturbation [21, 22].

When the acid-containing precipitation, in form of water, sleet, snow, or hail, falls onto the earth's surface, this phenomenon is named acid rain. These particles will have a pH level of less than 5.6. Acid rain has caused damages to lakes and other water sources, as well as forests and buildings.

They have also affected the marine ecosystem on a large scale. Figure 2-1 depicts the story of the impact of acid rain in two separate scenarios. On the left side image (Figure 2-1a), one of the seven wonders of the world, the Taj Mahal, has shown the deterioration caused by the emissions from nearby industries. When constructed, it was white but with industrialization and acid rain (a result of emissions from the nearby plant), the calcium from the marbles used has decomposed and has turned orange-ish in colour [19].

More than half of the geology of Canada is a hard rock (granite) based, which faces the damaging effects of acid rain. The right side image (Figure 2-1b) shows how Lake Ontario, one of the biggest water resources of Canada, like other water reservoirs, has also been affected. The water bodies in Canada lack natural alkalinity, like the lime base, which would act as the acid neutralizer and thus making them vulnerable. Provinces – Ontario, Quebec, New Brunswick, and Nova Scotia were the most affected ones as they are part of the Canadian Precambrian Shield [22].

Figure 2-1: Effect of Acid rain on a) Taj Mahal and b) Lake Ontario [19,23]

In order to fight the acid deposition problem, Canada created a federal-provincial team to coin a solution – the 1985 Eastern Canada Acid Rain Program. It was a science and monitoring program under which the eastern Canada cap of 2.3 million tonnes of SO_2 was to be met by 1994 and had to be maintained by 2000. Canadas also joined European nations and United State to sign the 1979 United Nations Economic Commission for Europe Convention on Long-Range Transboundary Air Pollution (UNECE LRTAP) and later sub-agreements on sulfur and nitrogen oxides. All the international agreements signed opened a gateway for the exchange of scientific and technical knowledge to counter the air pollution

In 1991, Canada-United States Air Quality Agreement was also signed which included specific commitments from both countries to:

- Cut SO_x and NO_x emissions,
- Ensure visibility protection,
- Prevent deterioration of clean areas and

- Conduct emissions monitoring.

Ongoing scientific research and monitoring led to many signed agreements and strategies to counter the SO_2 emissions. A more specific list of acts is shown below:

- Provincial/territorial regulations like the Ontario Regulation 397/01 on SO_2 and NO_x emissions caps and emissions trading
- Canadian Environmental Protection Act, 1999 (CEPA 1999) passed regulations for – sulfur in gasoline and diesel fuel, along with New Source Emission Guidelines for Thermal Electricity Generation (2003).
- Canadian Council of Ministers of the Environment (CCME) Sectoral Codes, Guidelines and Standards for Nitrogen Oxides (1991)
- Declaration of SO_2 and NO_x to be CEPA toxic (Government of Canada, 2003)
- Multi-pollutant Emission Reduction Analysis Foundation (MERAF) Reports for selected industrial sectors (CCME, 2003)

Several bodies like the Canadian Council of Ministers of the Environment (CCME) and Air Quality Committee (AQC) of the Canada-U.S. Air Quality Agreement (AQA) were also made to keep in check the rules [24,25]. All these agreements and efforts were successful in stopping SO_2 emissions increase and even start them decrease, but there is still a significant amount emitted every year.

2.2 Sources of SO_2

The major anthropogenic sources of SO_2 are the power plants and industries using sulfur-containing fuels like coal and oil as a source of energy. The combustion of fossil fuels, typically which contain 0.5-5% sulfur, has been widely used as a source of power for steaming the turbines

for electrical power generation, production of heat for concrete and paper industries, smelting of steel in steel industries and mineral ores [26].

The smelting of mineral ores and the oil refineries are other major sources of SO_2 emissions. First, during mining and mineral processing, the sources of SO_2 emissions are numerous. Exhaust from vehicles such as bulldozers, excavators, drills, and front-end loaders are some of the currently unavoidable emissions. These emissions not only release SO_2 but also pollutants like CO, NO_x, VOC, and PM [21].

Second, metals, when extracted from ores, are usually initially in the form of sulfide ores - iron, copper, zinc, lead, gold, and others. Thus, as a result of metal refining processes – mainly roasting and sintering stages – sulfur oxides are produced. For example, during the roasting of zinc ore, the ore is heated in presence of oxygen. Zinc oxide and sulfur oxides are then formed, as shown in equations 2.1 and 2.2. Approximately 93-97% of the sulfur from ore is then emitted as SO_x which accounts for around 90% of SO_x produced during the whole zinc processing [27].

$$2\,Zn + 3O_2 \rightarrow 2ZnO + SO_2 \qquad [2.1]$$

$$2SO_2 + O_2 \rightarrow 2\,SO_3 \qquad [2.2]$$

The pulp and paper industry is another important contributor to the emission of SO_2 and total reduced sulfur (TRS), which refers to a gaseous mixture of compounds containing one or more sulfur atoms in their reduced state, into the air [28]. The major sources are the recovery furnace due to the presence of sulfur in heavy black liquor, along with lime kiln and smelt dissolving tanks. The operating conditions of the recovery boiler will govern the SO_2 emissions. If the temperature in the lower furnace is sufficiently high, the SO_2 concentration in the flue gas can virtually approach zero. Whereas for lime kilns, the use of electrostatic precipitators and wet scrubbers to

capture lime dust along with the usage of low sulfur content fuel is one of the important mitigation solutions to decrease the emissions from this industry [29,30].

Figure 2-2 shows the total SO_2 emissions by various sources in Canada from 1990 to 2017. There has been a 69% reduction in the amount of SO_2 emissions produced between 1990 to 2017. During the year 2017, the largest amount, counting for around 40% of total SO_2 emissions, came from ore and mineral industries, of which 71% was contributed by the non-ferrous smelting and refining industry. Emissions from oil and gas industries, followed by electric utilities, accounted respectively for around 27% and 26% of the total emissions [31].

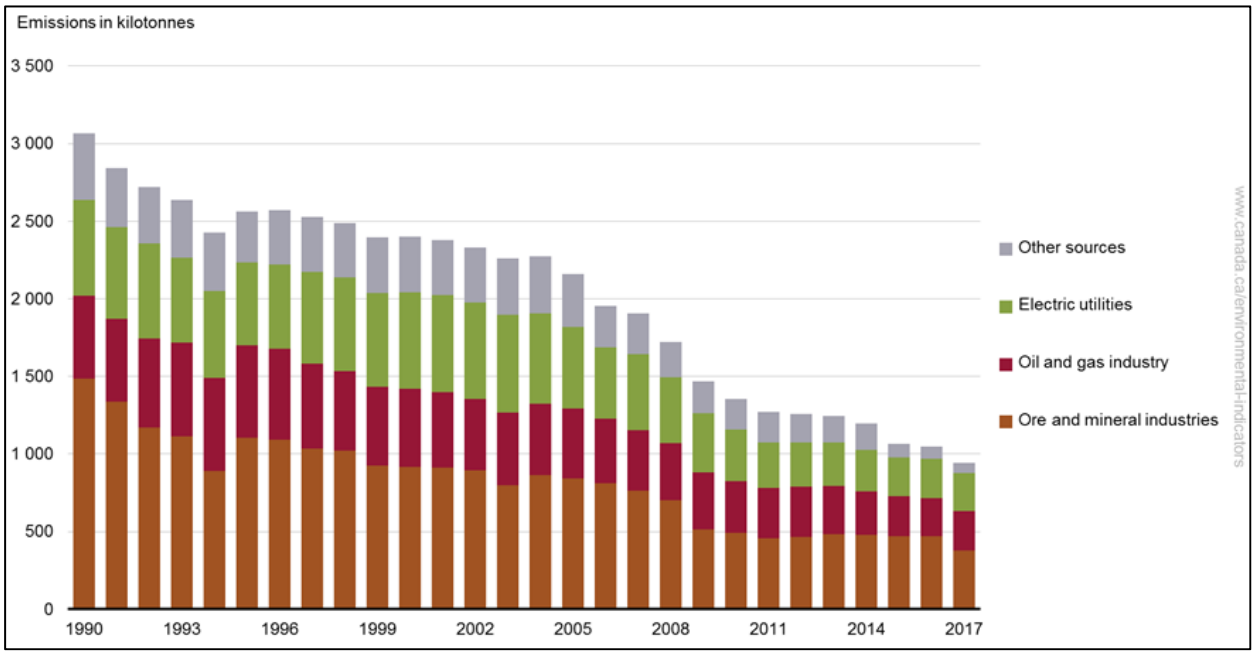

Figure 2-2: Total SO_2 emissions by sources, Canada, 1990 to 2017 [31]

This significant decrease in SO_2 emissions was due to actions taken and rules introduced by the government to act against acid rain previously mentioned. The technological upgrades, new air

pollution controls, implementation of regulations on low-sulfur fuels have also played an important role in reducing SO_2 emissions.

2.3 Removal and Capture of SO_2

To reduce the severity of SO_2 on the environment, a few methods have been used. The chosen methods for a given process depend upon factors such as space limitation, operation and maintenance costs, treatment of by-products, temperature and pressure of the reaction, and presence of water, other chemicals, and additives. Hanif *et al.* have listed a few methods which are actively utilized for the reduction of SO_2 emissions, summarized with main advantages and disadvantages in Table 2-1 [26,30].

Table 2-1:- Summary of methods utilized for reducing SO_2 emissions adapted from Mochida *et al* [26,30]

Method	Advantages	Disadvantages
Cleaner Fuel	• Low sulfur content hence Low SO_2 emission	• Production cost is high and dependent on the finite resource
Sulfur recovery unit	• Produces saleable sulfur	• Corrosion of the treatment equipment; requires a rich H_2S stream
Flue gas desulfurization (FGD)	• High removal efficiency (wet method), recycling of sorbent, and reduction in waste handling	• Wet method: the large area is required, high water consumption and generation of large solid waste. • Dry method: lower removal efficiency compared to the wet method
Coal washing	• Direct reduction of SO_2 emission; combustion of fuel is longer	• High operational cost and due to fuel alteration, the possibility of high operational cost

2.3.1 Flue Gas Desulfurization

FGD is the most well-known process and is used widely to mitigate the SO_2 emissions at the industrial level as it can achieve high desulfurization capacity (>99% by wet method FGD). Due

to the presence of a wide range of processes within FGD from dry FGD to wet FGD, a wide range of sorbents, which are mostly calcium and sodium-based, are used [26].

The study of FGD has been the focus since the 20th century. The research journey started from the SO_2 catalytic oxidation method to absorption in lime/limestone slurries. The areas focused on water scrubbing, metal ion solutions, dry adsorption, wet lime/limestone scrubbing, double alkali process, ammonia scrubbing, and processes based on SO_2 reduction [33].

FGD has a wide spectrum as it can be categorized into 3 basic types depending on the sorbent condition as Wet FGD, Semi-dry FGD, and Dry FGD. These can be further sorted based on the life cycle of the sorbent used as once-through and regenerable types. Figure 2-3 shows some of the different types of FGD.

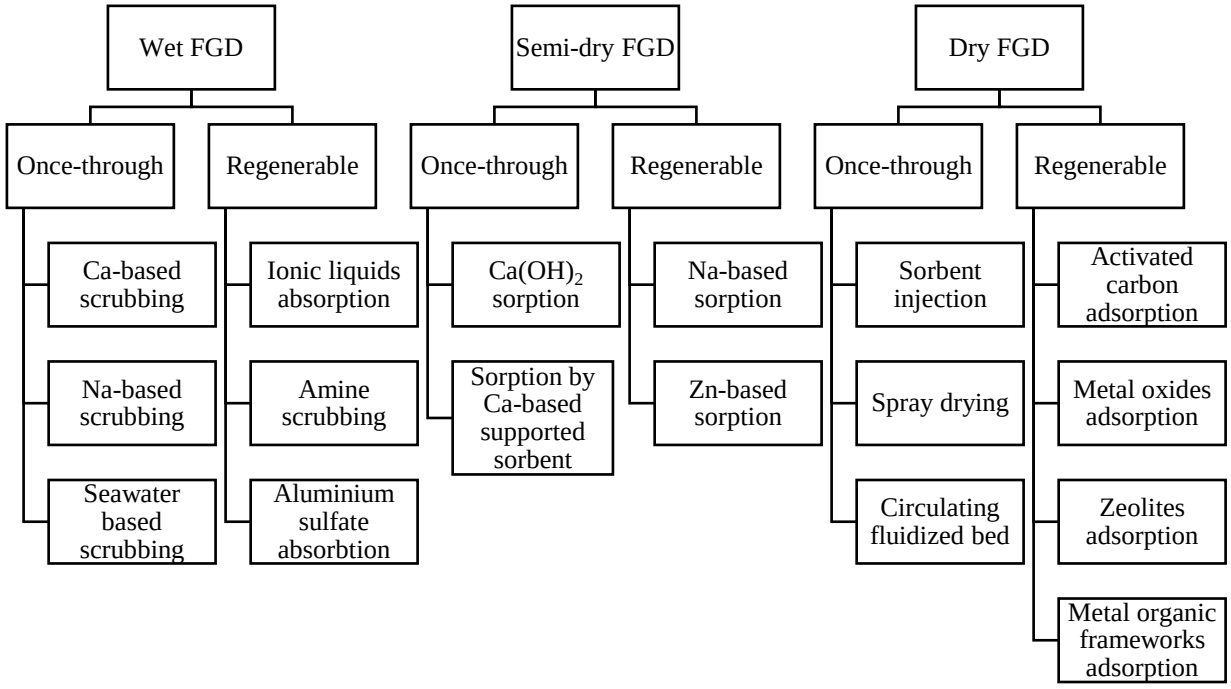

Figure 2-3: Schematic chart showing different types of FGD and their characteristics with sorbents used, adapted from Mochida *et al.* and Hanif *et al.* [26,32].

Sorbent regeneration and selection of method

The *once-through* type method which involves scrubbing with lime or limestone is widely used because of its high SO_2 removal efficiency. However, the spent sorbent cannot always be recycled and is often rather disposed of, creating a quantity of waste. It can sometimes be marketable, being utilized as the by-product – gypsum. For the *regeneration* type methods, the spent sorbent is regenerated, by removing/releasing SO_2 in elemental sulfur, gaseous SO_2, or sulfuric acid by chemical or thermal treatment of the sorbent. The sorbent can then be recycled for several sorption/desorption cycles until its removal capability gradually deteriorates. One of the disadvantages is the additional operational cost but would counter-balance the waste disposal problem of the *once-through* methods [26,32].

On the industrial scale, the selection of appropriate FGD depends on many factors such as the location of the plant, accessible resources, reaction parameters (concentration of SO_2, reaction temperature, the composition of flue gas), and by-product handling. For a lower concentration of SO_2 like in coal-fired plant– the once-through method is the appropriate one, whereas in high SO_2 content plants like mineral/ore processing unit – regenerative FGD would be the best one.

The total costs of the FGD use are also one of the main deciding factors. The combined capital, operation, and management costs of the FGD are in the order of dry < semi-dry < wet. The usage of water is the main reason behind this order [26,33].

Wet FGD

The sorbents used in wet FGD are in the form of a slurry. This process possesses the highest efficiency among all the types of FGD techniques used. A schematic of wet-flue gas desulfurization is shown in Figure 2-4.

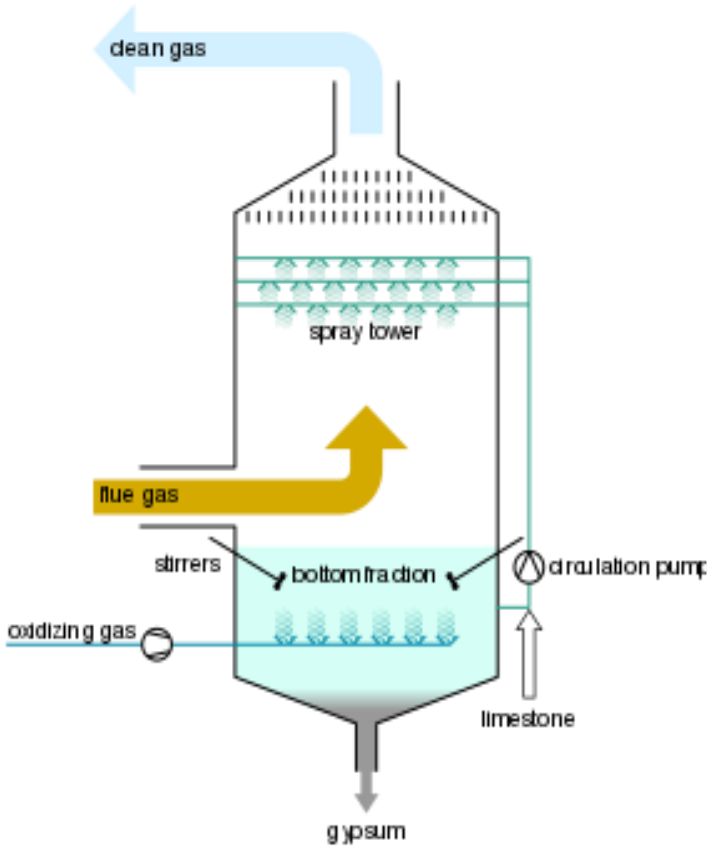

Figure 2-4 Schematic of Wet Flue Gas Desulfurization Unit [36].

The major drawback is majorly the formation of moisture saturated flue gas and wastewater. These demand proper disposal capital have a high capital cost for the water purifier units and the moisture in the flue gas facilitates corrosion which in turn adds to the capital along with big installation

units over large areas which are difficult to be integrated into old plants. The by-product -gypsum is also difficult to dispose of when there is little or no demand for it.

Dry FGD

This process uses solids, powder, and pellets, for the adsorption of the flue gases. The flue gas is low in moisture and waste and by-products are in solid form which makes the disposal easier. But the SO_2 removal efficiency is lower than wet FGD.

Semi-dry FGD

It is a combination of both Wet and Dry FGDs. The dry sorbents are utilized to the full extent as the fluids are injected at intervals to heighten SO_2 adsorbate and sorbent interactions during reactions. The production of dry by-products helps in easy disposal. It has a higher removal efficiency than Dry FGD but lower than Wet FGD [6,32].

Advancement in technologies

When SO_2 concentrations are higher, wet FGD is preferred because it has higher efficiency and a high utilization rate of limestone [34]. In wet FGD, the SO_2 containing flue gas encounters alkaline slurry (usually lime or limestone slurry) which acts as an absorber. The reaction tank holds the absorber effluent and provides enough retention time for finely grounded lime/limestone particles to dissolve and react with thus dissolved SO_2. The spray tower is vertically suspended which provides countercurrent flow of the absorber to increase the rate and efficiency of SO_2 removal. To prevent scaling problems caused due to the by-product of the reaction, gypsum, the air is blown into the limestone slurry to promote the oxidation process. Sometimes to control the oxidation process, sodium thiosulfate ($Na_2S_2O_3$) is added to the reaction tank. This prevents oxidation from gypsum as it lowers the slurry oxidation ratio below 15% [17].

To compensate for the cost of installation, researchers have tried enhancing the reactivity of lime and decrease the running cost of the spray dryer system. The additives like fly-ash and sodium hydroxide are added to lime for increasing the reaction time and the effects of humidity in the duct are also been examined [34].

The reliability of the FGD process was summarized by Miszczyk, A., and Darowicki, K. They concluded that due to very aggressive corrosion conditions inside the FGD tower, stainless steel and alloys containing a significant amount of chromium, nickel, or titanium should be used. Application of thermal insulations on the ducts of the scrubber that would help to ensure that the temperature of the flue gas does not decrease below the dew-point of sulfuric acid and to avoid corrosion problems was also recommended [37].

Thus, even though FGD provides good efficiency of SO_2 removal, there are important disadvantages. These disadvantages are high operational cost, high water usability, high energy consumption, waste production, and large land area. They are enough to give it a second thought before installation in an industrial plant.

2.3.2 Adsorption using zeolites and Metal Oxide Frameworks

The adsorption of SO_2 on the surface of porous solid materials, zeolites, Metal Oxides (MO), Metal-Organic Frameworks (MOFs), or activated carbon, presents a potentially cost-effective alternative to the current state-of-the-art SO_2 removal technologies discussed above. This section will provide an overview of both, traditional and emerging, adsorbent materials that have been tested for SO_2.

The removal of SO_2 by adsorption could be an interesting alternative because even at high inlet concentrations, high efficiency can be achieved. In addition, process unit design is usually simple,

as of its operation. However, when applied at a large scale, high financial costs and huge equipment could play as drawbacks [38].

The main adsorbents presently studied and used on a large scale are zeolites, MOFs, and metals and/metal oxides. A brief overview of the adsorbents is presented further in the following sub-sections.

Zeolites

Zeolites are crystalline aluminosilicates and are often used for molecular separations and reactions because of well-defined pore structure and exceptional surface properties as well as generally regenerable. Natural and synthetic zeolites are widely used in applications such as catalysts, adsorbents, and membranes [38]. An example is given in Figure 2-5, a zeolite framework where Co is bound to three O atoms in a six-ring unit along with a bond of nitrogen of a bent mononitrosyl ligand. Oxygen atoms of the zeolite framework are shown smaller than the NO oxygen for clarity [39].

The zeolites could be used in a fixed bed configuration. They can selectively adsorb molecules that have a smaller pore size than that of the zeolites (~7 Å). SO_2, which has a diameter of about 3.7 Å is likely to be adsorbed on all surfaces of the zeolites [40]. Zeolites could also be a substitute as well in lime-based scrubbing, which can reduce transportation and disposal costs of lime, as well as reduce fly ash disposal to a certain extent. This is because the loaded zeolites could be processed to recover the SO_2 gas and then used as soil conditioners [6].

Zeolite X, Zeolite Y, and silicate have been explored for SO_2 capture with promising results. Kopac and co-workers investigated molecular sieve 13X for SO_2 adsorption over 250-400℃ and achieved significant adsorption capacity at 250℃ [3,39]. Marcu *et al*, studied the SO_2 adsorption on Y

zeolite and found that the activity remains constant during the 20 adsorption-desorption-regeneration cycles [42]. Zeolite 4A showed higher SO_2 adsorption capacity over zeolite 5A when investigated by Kopac and co-workers over the temperature range of 250-445 °C [41]. Fly ash zeolites such as Zeolite X, zeolite Y, NA-P1, analcime, and sodalite removed 2000 ppm SO_2 when experimented with a simulated gas at room temperature [3,39].

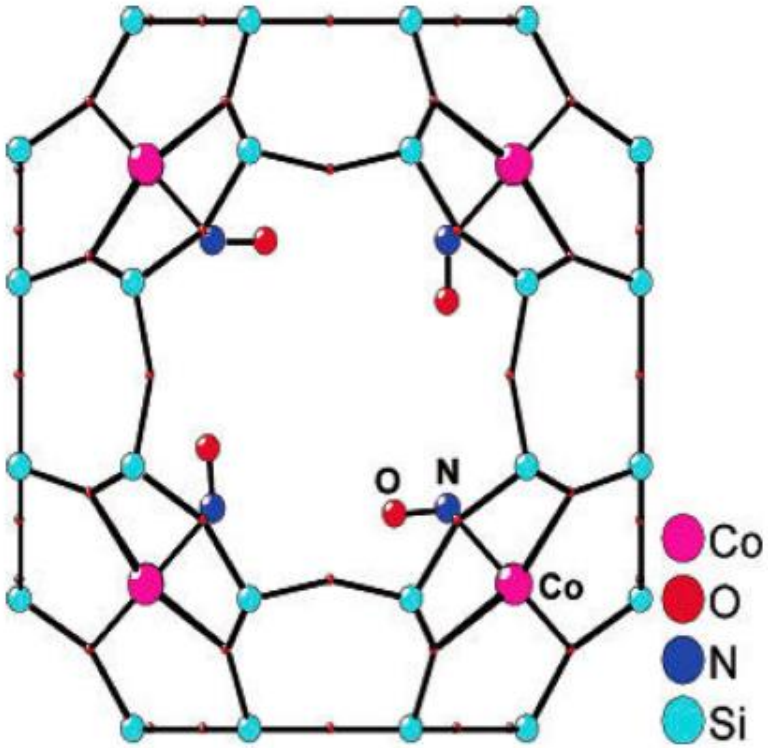

Figure 2-5: Structure of cobalt-NO complex in Zeolite A, revealed by single-crystal XRD [39]

Alver *et al.* conducted the adsorption experiment of SO_2 onto the clinoptilolite-rich zeolite tuff from Gördes (Turkey). The natural form and it's cation-exchanged (Na^+, K^+, Ca^{2+}, and Mg^{2+}) form were investigated up to 100 kPa pressure at two different temperatures (273 K and 293 K). The quantitative analysis showed that the uptake of SO_2 onto the synthesized and natural zeolite

adsorbents increased in the order of Ca-G < natural-G < Mg-G < K-G < Na-G at both temperatures [43].

The adsorption temperature and the SO_2 concentration are the key factors influencing the adsorption capacity for zeolites [42], but gas moisture is also important. Muhammad *et al.* retained their stability in the dry gas environment but when exposed to moisture the adsorption was weakened. At high temperatures (400°C and 650°C) interaction with SO_2 destroys their framework which in turn affects their adsorptive behaviour. Even though they can be regenerated multiple times, but their application is limited because of low adsorptive site density and limitations in the pore size [26].

Metal-Organic Framework

MOFs are 3D materials composed of metal ions in clusters that are linked together by organic compounds or linkers by strong covalent bonds (Figure 2-6). They have customizable surface functionalities and extraordinary high surface areas [26,32]. Metals usually used for MOF synthesis are Zn, Cu, Mg, Co, Cd, Zr, Ti, Ln, etc. as these can adopt various geometries – tetrahedral, square, octahedral, etc. Commonly used synthesis methods for MOFs are – hydrothermal, solvothermal, ultrasonic, and microwave methods [26].

They are potential candidates for SO_2 capture as Their sorption capacities are better when compared to the dry sorbents [26].

At high temperatures, Benzenetricarboxylate MOFs with copper as the central cation and $BaCl_2$ as a second component (Ba/Cu-BTC) for SO_2 adsorption and showed increased uptake at high temperatures [26,32]. Fluorinated MOF (FMOF-2) synthesized from 2,2-bis (4- carboxyphenyl)

hexafluoropropane and zinc nitrate hexahydrate were showed to have a high adsorption capacity and selectivity for SO_2 in a mixture of SO_2, N_2, and CH_4 [26,32].

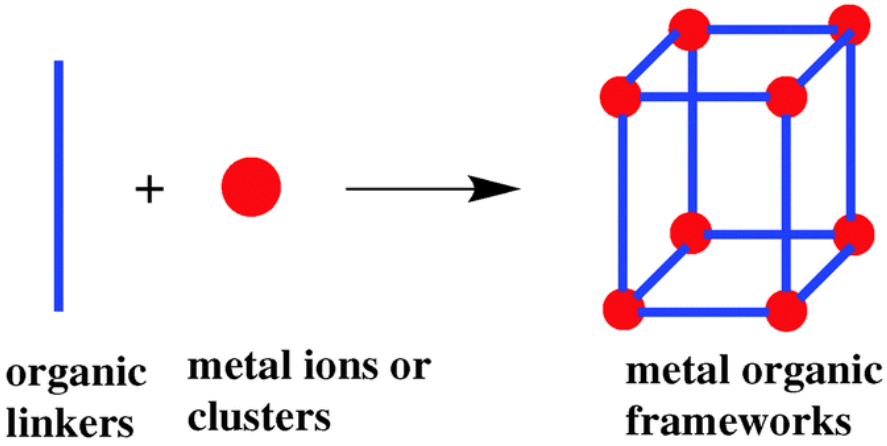

Figure 2-6: Structure of Metal-Organic framework [44].

The major drawback of using MOF adsorbents is the instability of the coordination compounds of MOFs on exposure to wet flue gas [45]. They suffer from corrosive and toxic properties of SO_2 which result in structural damage and irreversible SO_2 uptake. Also, the high cost of the organic precursors of MOFs has limited its applications [46,26].

Post-synthetic modifications of MOFs to ensure their stability when exposed to a humid environment and increase of the sorption capacities are the main focuses of the researchers [3,47]

2.3.3 Metals and metal oxides

Application of metal-based catalysts as adsorbents for the capture of SO_2, is used and studied because of its high possible desulfurization efficiency, but generally at high temperature. The frequently used catalysts would be metal oxides or mixed metal oxides, primarily of transition metals due to their low production cost, selective action, and easy generation [26]. These metal

oxides are primarily obtained from naturally occurring metallic oxides or laboratory synthesis of metallic salt precursors, by co-precipitation or hydrothermal method [26].

SO_2 abatement using metal oxides apart from CaO has been extensively delved into [3]. The naturally obtained metal oxides like iron oxide, carbonates such as limestone which can be used to synthesize CaO, showed high removal of SO_2 efficiency. However, the application of high heat during calcination added important operational costs [26]. Mathieu *et al.* classified the metal oxides into 3 main categories – single oxides, mixed oxides, and supported oxides. It was concluded that silica-based adsorbents were more promising ones due to high surface areas and inertness of silica towards SO_2. The problem posed by metal oxides was the formation of stable metal salts on exposure to SO_2 leading to rapid deactivation and hence decreasing in the SO_2 removal capacity [3,48].

McCrea, D. H. *et al.* conducted experiments with CuO and SO_2, with the series reactions shown in equations 2.3 and 2.4. They concluded that that the conversion would complete at temperatures lower than 450℃ [3,49]. The regeneration was possible at higher temperatures (around 700℃), but with the possibility of the formation of methane and carbon dioxide.

$$CuO + SO_2 + \frac{1}{2}O_2 \rightarrow CuSO_4 \quad [2.3]$$

$$CuSO_4 \rightarrow CuO + SO_2 \quad [2.4]$$

The experimental studies of the reaction of SO_2 with iron oxides and aluminum oxides suggested that they capture with metallic oxides occurs through a mechanism involving the production of sulfite or sulfate salts. The role of the surface hydroxyls, which were suggested as the active sites for SO_2 adsorption and oxidation, remains unclear. However, these surface hydroxyls when comes

in contact with the dissociated water molecules, form interfacial hydroxyl groups whose reactivity generally depends on the electronic properties and cell geometries [50].

H.Wu, *et al*., used MnO_2 to demonstrate efficient adsorption and oxidation of the surface-bound sulfate and have put forth MnO_2 as a strong candidate for SO_2 capture [51]. When they investigated the mechanism, the terminal hydroxyls were found to have high reactivity associate with SO_2. The regeneration was conducted by a conventional electrochemical process resulting in the conversion of sulfate to sulfuric acid [3,46].

Thus, the presence of oxygen sites on the metal oxides has enhanced the reactivity of the solid surface with the gas but the application of high temperatures might lead to deactivation [3,46].

2.4 Carbon-based Materials

The versatility and characteristic of carbon-based materials make them a good candidate for adsorption applications in general but also for SO_2 capture. Resistance to acidic and basic environments, low cost, low density, recycle capabilities, abundant micropores, easy synthesis processes, affinity with compounds, regenerability, mechanical strength, diffusion characteristics, stability, and availability are some important characteristics that have been researching to date. Activated carbon, carbon monoliths, carbon nanotubes, graphene-based products are the most popular examples of carbon-based products which have been actively investigated to explore their applications in various fields [47,48,49,50].

2.4.1 Activated Carbon

Activated carbon is a microcrystalline form of carbon with high surface area and high porosity. It is widely used to remove impurities from solid-liquid and gases. It can be easily synthesized from a variety of raw materials like coal, wood, fly ash, coconut shell. The carbon activation process

involves raw material preparation, low-temperature combustion, and calcination for activation. Main industrial applications are catalyst or catalyst support, gas adsorbent, water purification, and molecular sieves. The difficulty in the mass transport process and a wide range of pore sizes resulted in low adsorptivity [56]. This resulted in a low catalytic activity, which was overcome by loading active components on the surface of AC in the form of metals/metal oxides [47,32].

For SO_2 adsorption, the porous structure and the surface chemistry of the AC are important parameters. Raimundo-Piñero *et al.* suggested that SO_2 oxidation to SO_3, a probable adsorption mechanism in AC, is highly influenced by the pore size distribution, and the optimum pore size which favored oxidation of SO_2 to SO_3 would be 0.7 mm [57]. On the other hand, Daley *et al.* mentioned that an increase in the SO_2 adsorption capacity of AC fibers after the oxygen surface groups were removed by heat-treatment in an inert atmosphere. The reason was reported to be the increase in the carbon-free sites for SO_2 oxidation which were the result of the decomposition of oxygen-containing functional groups during the thermal treatment.

Two different kinds of AC – granulated activated carbon and PAN fiber – were used by Martine *et al.* to test the SO_2 capture with SO_2 lower than 100 ppm [52],[58]. The granulated AC trapped SO_2 in the air at a concentration as low as 2.5 ppm, but the amount of SO_2 adsorbed per gram of AC decreased when a high concentration of SO_2 in the air (>1000 ppm) was used. The adsorption of SO_2 was irreversible and was then followed by oxidation indicating the mechanism was not physisorption.

Atanes *et al.* studied the SO_2 removal efficiency by adsorption on the activated carbon, which was synthesized by waste cork powder and chemically activated by potassium hydroxide. They found that the adsorption was promoted by a high surface area provided by the AC and also influenced by the surface basicity [59].

The removal of SO_2 using AC fiber in the presence of O_2 and H_2O was studied by Gaur *et al.*, to carry out the process without catalyst regeneration [54,55]. In the presence of O2 and H_2O, the adsorbed SO_2 was converted into H_2SO_4 on the AC surface. The SO_2 concentration levels at the steady-state at the outlet of the reactor increased with an increase in inlet SO_2 concentration and decreased with an increase in the oxygen and water concentration levels. The best results were at 40℃ with the O_2 and H_2O concentrations as 20% and 30% (v/v) respectively. Above this temperature, gradual degradation of catalytic activity was noted. The whole process was diffusion or kinetics controlled with the maximum limit value of $D_{eff} = 5.2*10^{-10}$ m^2/s, with diffusion below this value and kinetics above it. The rate-determining step in the kinetics controlled part was the desorption of the product (sulfuric acid) from the surface. Thus, with the addition of oxygen and water into the reaction system at low temperatures, it has facilitated the SO_2 capture and the catalytic activity remained for a long duration (120 h) but is degraded at high temperatures [54,55].

Bing Li, et.al. studied the mechanisms of SO_2 adsorption/reaction by AC from flue gas. The SO_2 adsorption removal by AC was characterized as one kind of dry FGD where SO_2 was catalytically oxidized and hydrated into H_2SO_4 in the presence of O_2 and H_2O, where H_2SO_4 is stored into the pores of AC [56,32]. It is schematized in Figure 2-7.

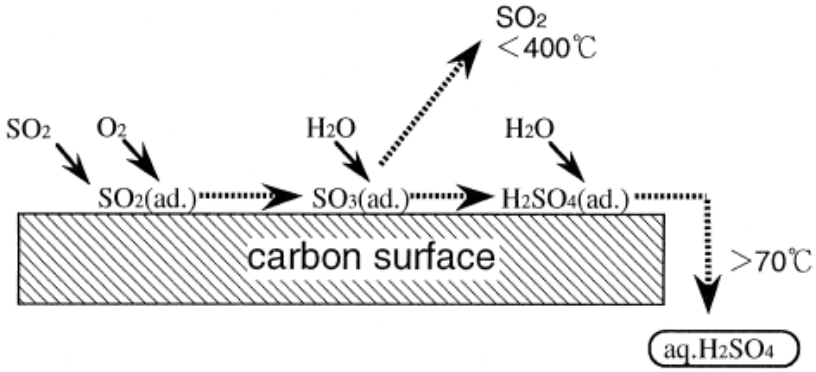

Figure 2-7: Capture of SO_2 on the surface of AC [34].

The following reaction mechanism (equations 2.5 to 2.10) for the adsorption of SO_2 by AC at 100℃ in the presence of oxygen and water was proposed by Tamura *et al.*[34].

$$SO_2 \rightarrow SO_{2(\text{ad})} \quad [2.5]$$

$$H_2O \rightarrow H_2O_{(adO)} \quad [2.6]$$

$$\frac{1}{2}O_2 \rightarrow O_{(ad)} \quad [2.7]$$

$$SO_2 + O_{(ad)} \rightarrow SO_{3\,(ad)} \quad [2.8]$$

$$SO_{3(ad)} + H_2O_{(ad)} \rightarrow H_2SO_{4(ad)} \quad [2.9]$$

$$H_2SO_{4(ad)} + nH_2O_{(ad)} \rightarrow H_2SO_4.nH_2O_{(ad)} \quad [2.10]$$

On exploring the mechanism, they found that with an increase in SO_2 concentration at the inlet of the reactor, the initial SO_2 adsorption rate increased but with an increase in adsorption temperature, the rate of adsorption decreased, typical of physical adsorption [34]. Hanif *et. al.* also supported

this by stating that this inability, has lowered the SO_2 adsorption capacity and the breakthrough time has shortened, resulting in weak selectivity [26]. They also added that even a low concentration of acidic gas in the inlet will lead to low adsorption capacity. Hence, AC is unable to withstand high temperatures and cannot be a good adsorbent at low SO_2 concentrations [26].

Two main ways are proposed for the regeneration AC used for SO_2 capture depending on the application and sulfur species on the surface. There are the hydration and elution of sulfuric acid or the reduction of SO_3 to SO_2 over carbon. The regeneration of SO_2 adsorbed AC was tried by Yamamoto *et al.* and Gupner, and Mauvin *et al.* by water scrubbing [6,32]. However, the process required a large amount of water as strongly adsorbed H_2SO_4 in the pores of AC tends to remain bonded even after rigorous washing, prohibiting complete regeneration. Regeneration by heating (around 400℃) was also tried by consuming part of the surface carbon. The carbon sacrificed during this regeneration usually sustain oxygen functional groups and is decomposed to CO_2 (400℃) and CO (800℃). Though this resulted in the loss of mechanical strength and a decrease in the amount of surface oxygen.

Mochida *et al.* explored the recovery of sulfuric acid by sufficient hydration. Better extraction efficiency was obtained when the condensation of steam in the pores method was applied rather than by liquid water. Thus, a lower temperature for regeneration is preferred [34].

Hybrid catalyst-adsorbent systems have been explored using various metal oxides such as V_2O_5, CuO, Fe_2O_3, MnO_2, Cr_2O_3, and CeO_2 deposited on the surface of AC [3]. When tested at low temps for solely SO_2 removal, V_2O_5-AC was found to be the best candidate. When tested for simultaneous removal of SO_x and NO_x removal V_2O_5-AC and CuO-AC was found to be a most promising candidate as it displayed high removal efficiency at high temperatures 485-547℃, 88%, and 74% respectively [62].

2.4.2 Graphene Oxide for SO_2 capture

To investigate more on how the surface oxygen functionalities are contributing to SO_2 capture, few researchers have studied Graphene Oxide (GO). Isotherms were used to evaluate the initial heat of adsorption of SO_2 on GO and a valuer of 18 kJ/mol on GO flakes was obtained, hence indicating physisorption [55].

The oxidation of SO_2 to SO_3 by GO and GO foam was experimented in the liquid phase, with SO_2 gas bubbled through a water-GO suspension. The results reported by U. Burghaus *et al.* stated that the oxygen was consumed, and graphene acted as the catalyst [63]. The oxidation mechanism of SO_2 and H_2SO_3 on GO was then theoretically represented by DFT calculations. In the proposed mechanism, SO_2 reacts with epoxide-like oxygen groups on the surface of GO in a two-step process. The two C-O bonds by which the epoxide binds to GO are subsequently broken, beginning the process interestingly with the C-O bond farthest away from the approaching SO_2, followed by the breaking of the second C-O bond closest to SO_2. Synchronously formed is a new S-O bond transforming SO_2 to SO_3. This process is theoretically described as feasible even at room temperature [59,60].

When the reaction was performed with pristine graphene, the vacancy defects enhanced the SO_2 binding. The increase in the adsorption energy was associated with the hybridization between the S 2p orbital of SO_2 and C 2p orbital of graphene. SO_2 and metal (Al, Si, Pt) doped graphene showed strong chemisorption using DFT results [60,61].

2.4.3 SO_2 capture with sorbents

In summary, various materials are currently investigated for the capture of SO_2. If the targeted process is adsorption, it has been shown by studying the capture phenomena and the material – SO_2 interactions, that there are many possible mechanisms involving not just physisorption or even

chemisorption, but also surface reactions involving oxygenated functions and other gas components. Depending on the application temperature, the sorbent material, and the other gaseous components, behaviours vary greatly and as such involved mechanisms.

Moreover, some studies have shown that the affinity of SO_3 with the carbon surface is higher than for the SO_2 leading to possible greater capture capacity [67]. In addition, metal oxides and oxygen functions can participate in the oxidation of the SO_2 by either providing oxygen in the anoxic environment or catalyzing and promoting the oxygen transfer from the surface or the gas phase. A carbon-based material functionalized with metal could then be an adequate material providing sites for the reaction and sites for the adsorption.

2.5 Graphene Oxide

GO has been described as a monolayered structure from a bulk form called graphite oxide and attracted high interest. It possesses a 2-dimensional crystal structure of sp^2 hybridized carbon. These have been densely packed into a hexagonal honeycombed lattice. This structure provides GO with high tensile mechanical strength. The oxygenated functional groups decorated on the surface are hydroxyl and epoxy groups while the edges have carboxylic groups (Figure 2-8). The GO sheets are held together with hydrogen bonds which play an important role in dispersive behavior. Due to high mass transfer and intrinsic properties, GO is very useful in catalytic conversions [14,63].

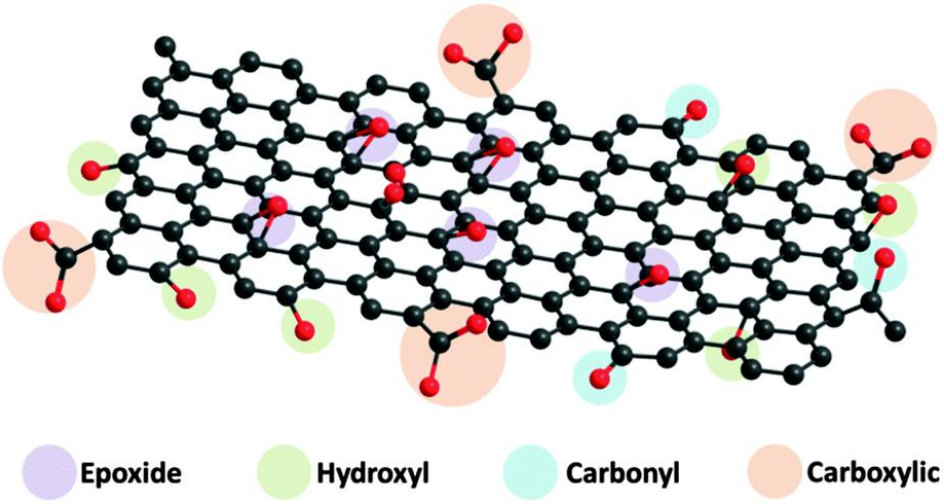

Figure 2-8: Structure of GO [69].

2.5.1 Methods of synthesis

The history of GO synthesis dates to 1859 when British chemist Brodie explored the structure of graphite by performing reactions involving strong oxidizing agent – potash of chlorate ($KClO_3$) and nitric acid (HNO_3). Brodie found thus synthesized material dispersible in water and alkaline medium and high in oxygen content [14]. Nearly 40 years later, L. Staudenmaier improved Brodie's method by adding $KClO_3$ in intervals rather than at once and the addition of H_2SO_4 to the reaction. This slight change resulted in an increase in overall oxygen content in a single approach rather than multiple oxidations making it more facile.

60 years later, in 1958 Hummers and Offeman developed an alternative method by reacting graphite with potassium permanganate and sulfuric acid and achieved the same levels of oxidation. Though this method has been modified with time and is now commonly used and referred to as the Modified Hummers Method [70,71].

The change in the oxidizing agents has related to safety concerns and the extent of heat released during the reaction. Nitric acid, a common oxidizing agent is known to strongly react with carbon

compounds. The reaction liberates gases like nitrogen oxides (NO_2 and N_2O_2) and some chlorine oxide (ClO_2) which is released as a by-product. These gases are explosive hence a controlled environment is required during the synthesis. The Hummers method combined strong but comparatively safe oxidants: potassium permanganate and sulfuric acid.

The active component during the reaction is the diamanganese heptoxide formed by the reaction of $KMnO_4$ and H_2SO_4. The bimetallic heptoxide selectively oxidizes unsaturated aliphatic double bonds (Tromel and Russ) which provides a look into the reaction pathway [72]. The modified Hummers method then combines strong oxidants – $KMNO_4$, H_2SO_4, and H_2O_2 with graphite flakes (widely available source of graphite) within a temperature-controlled environment [14].

One of the main issues faced by researchers for large-scale production of GO is the safety of the method. Despite the modifications made in the traditional Hummers methods, the control of temperature throughout the experiment has been proven troublesome. Marcano *et al.* used the combination of phosphoric acid and sulfuric acid of 9:1, trying to double the mass of $KMnO_4$, but the temperature control was left in dark [73].

2.5.2 Characteristics and Properties

A common feature of all the methods was the strong oxidation of graphite to different levels. During these processes, functional groups such as hydroxyl groups (OH), carboxyl groups (COOH) are introduced on the material, hence increasing the d-spacing [71,16].

On performing nuclear magnetic resonance (NMR) Ruoff and co-workers found that epoxy and hydroxyl groups are two major functional groups across the basal plane and are located close to each other. Minor peaks also revealed the presence of lactols, ester carbonyl, and ketone groups,

[14,65,66]. On performing x-ray photoelectron spectroscopy (XPS), sp^2 C in aromatic rings and C atoms bonded to hydroxyl, epoxy carbonyl, and carboxylic groups were discovered [1,14,66,67].

Erickson *et al.* differentiated three major regions by transmission electron microscopy (TEM): holes, graphitic regions, and high contrast disordered regions. Holes were proposed to be the result of the evolution of CO and CO_2 during the reaction; Graphitic regions to be the result of incomplete oxidation of the basal plane and the reason of the preserved the honeycomb structure of graphene; the disordered regions to be due to abundance of oxygen-containing groups namely hydroxyls, epoxies, and carbonyls.

Graphene oxide's structure and composition were continuously further explored. The presence of hydrogen bonds in between layers was related to its hydrophilic properties. High-resolution TEM by Gomez- Navarro *et al.* highlighted topological defects in GO such as a cluster of pentagons and heptagons were surrounding GO lattice along with some in-plane distortions and strain.

Pandey *et al.* on performing scanning tunneling microscopy (STM) on the oxygen groups observed a periodic arrangement of O over a few nanometers which were arranged in the form of rectangular lattice implying strips of epoxy groups [14,68,69].

Properties

Graphene oxides, therefore, have numerous very interesting properties due to their characteristics.

- Electronic properties: GO has a large bandgap but the electronic properties can be tuned. The electronic properties depend on the structural disorder of the material, precisely the structural disorder of the sp^2 bonding network to sp^3 hybridized bonding. This can be restored by reducing GO to rGO using either chemical, thermal, or electrochemical methods [14,70].

- Dispersibility: GO can be easily dispersed in water and polar organic solvents like ethylene glycol, N, N-Dimethylformamide. The high dispersion is due to the easy reactivity of GO with a solvent which results in greater polarity hence good dispersibility [14,71].
- High Surface area: GO has an extremely high surface area (~ 2630 m^2g^{-1}) [14,70].
- Thermodynamic stability: GO is unstable above 80℃ and slowly starts to decompose. If the temperature exceeds 120℃, GO tends to decompose rather rapidly. The thermodynamic stability relies on the geometric structure and chemical stoichiometry. Thus, a completely oxidized GO will be thermodynamically stable as the coverage functional groups lower the formation energy as indicated by Wang *et al.*[14,72]
- Mechanical property: Graphite oxide has Young's modulus of 6-42 GPa and as the thickness is reduced, Young's modulus will significantly increase thus giving the monolayered GO a high tensile strength with Young's modulus of 250 ± 150 GPa [14,73]

2.5.3 Applications

In recent times, many studies are revolving around GO and the demand for high-grade GO over the years has increased due to the versatility of GO in a wide range of applications, in addition to sorption (section 2.4.2) and catalytic applications (section 2.6). Here are few examples of the variety of current research and technology improvements to show the versatility of the material.

GO has been actively used in electronic devices as sensors or the form of reduced GO. The multilayer material film has been applied in coating technology as it is optically transparent and impermeable under dry conditions. GO reacts actively with many polymers to form nanocomposite which boosts up the properties of the original polymer including tensile strength, elastic modulus, electrical conductivity [14,70].

GO has been playing an active role in optoelectronics, either as bio-devices or as drug delivery material functionalized with the amine. Several electronic devices are fabricated with GO as the starting material for example field effect transistor which is used as a chemical and biochemical sensor to detect the hormonal catecholamine molecules, avidin, and DNA. One of the major application areas of the GO is in the production of transparent conductive films by depositing them on the substrate. Such coatings are used in solar cells, flexible electronic devices, chemical sensors, etc. [14,71].

With an extremely high surface area (~2630 m^2g^{-1}), GO can be used for energy storage such as in Lithium batteries, double-layered capacitors as well as fuel cells and solar cells. Besides these, GO possess potential fluorescent properties that can be used in biosensors for the detection of early diseases and even can assist in drug development for cancer and biologically relevant diseases. GO structures swell up when water is permeated through the membrane which enables the formation of a water penetration path between the layers of GO. It can also be used in cation exchange membranes like KCl, HCl, etc. which have applications in water desalination [14,52,72].

GO is used as a precursor for thermal dissipation films. The GO membranes are converted into high-grade 'graphite-like' membranes by a heat treatment up to 2800 °C. The in-plane thermal conductivity of such 'graphite from graphene oxide' is as high as 1500 W/mK, close to that of graphite films made from polyimide films. The high thermal conductivity has made it possible for the heat dissipated GO films to be applied in mobile electronics such as mobile phones or pads, with potential use in laptops and other devices in the future [14,40,71].

GO was investigated for catalytic application and has attracted attention for converting air pollutants into useful energy sources. With tetrabutylammonium bromide as a co-catalyst, GO-Bu_4NBr converts CO_2 into propylene oxide with 96% yield under mild condition [84]. The

oxidation of SO_2 to SO_3 on porous GO [85], the Fisher-Tropsch CO_2 hydrogenation process on GO-Co catalyst[86] catalytic conversion of CO, CO_2, and NH_3 with GO being used as a support are some of the examples of application for removal of air pollutants [79,13].

Similarly, owing to the presence of oxygenated groups on GO surface as the active sites and structural stability, GO had displayed promising removal capacity heavy metal ions through adsorption of Cu^{2+} ions (yang 2010), Cd (II). Co (II), Au (III), Pt (IV) and Pd (II) ions [88], [89]. In addition, the GO also exhibited high removal efficiency of organic dyes [82,13].

Finally, combining polymers with graphene oxide for fabricating low-density nanocomposites, with exceptionally high mechanical properties, has gained importance in the various research fields [91].

2.6 Graphene Oxide Functionalization

GO has been considered as attractive catalytic support because it enhances the catalytic properties of metal and metal oxide nanoparticles. The extremely high surface area (~2600 m^2/g), good chemical stability, high thermal and electrical conductivity, and high performance to protect the catalyst through the sp^2 hybrid 2D carbon network [92]. The electron transfer from GO during the reaction can promote electron transfer. When used as support for the metal nanocatalysts, it enhances the reduction efficiency for the whole GO-nano composite together [92].

Kaiqiang Zhang *et al.* used a facile hydrothermal self-assembly method for the synthesis of an efficient nanocomposite catalyst consist of graphene oxide (GO) supported copper oxide nanoparticles (CuO–GO). The thus synthesized CuO–GO nanocomposite catalyst demonstrated a high yield for the reduction of a variety of nitroaromatics in aqueous sodium borohydride ($NaBH_4$) at room temperature. High catalytic activity was reported and related to the synergistic coupling

effect of Cu when coupled with the GO nanocomposite catalyst. They used the CuO-GO nanocomposite catalyst, for the reduction of 4-nitrotoluene, for six consecutive cycles with a good yield of 85% (for the last one) [83,85].

Shabestari *et al.* decorated the surface of GO with various double salts of CuO and metallic copper: copper nitrate, copper hydroxy nitrate double salt (DS) ($Cu_2(OH)_3(NO_3)$), copper (II), and copper (I) oxides and metallic copper (Cu_0). They studied their catalytic activity for different coupling reaction systems such as the catalytic oxidation of benzyl alcohol, the catalytic Suzuki C-C coupling reactions, and the catalytic C-S coupling reactions. For the reaction of 4-iodoanisole with benzylamine, they concluded that copper double salt GO composite was the most active material because of its high surface area, the better dispersion, and the increased basicity (because of the presence of hydroxyl group), which played a major role in the coupling reaction [92].

The application of GO-Iron oxide composites as adsorbents for wastewater treatment is also studied. Fe_3O_4/GO nanocomposites, prepared by impregnation and co-precipitation were tested against rapid removal of organic antibiotic pollutants (tetracycline, oxytetracycline, chlortetracycline, and doxycycline) from aqueous solution. The experiment showed high efficiency for low levels of antibiotics in large volumes of water and was then applied to Pearl River water [86,84].

Zhao *et al.* and I. Ali *et al.* studied GO impregnate with iron oxide nanoparticles for the removal of atrazine from an aqueous medium and found a moderate removal capacity [75,95].

On further research presented by Andrade et. al., where they synthesized GO@α-γ-Fe_2O_3, they recorded 42.5 mg/g adsorption capacity of atrazine with 71% removal a 45°C. A pseudo-second-

order reaction model presented as the best fit for the kinetic data, suggesting the chemisorption process of the adsorption [92].

Santos *et al.* also studied the α-γ-Fe_2O_3 – GO composite for removal of glyphosate. A simple deposition of α-γ-Fe_2O_3 on GO by using ultrasonication with propanol as a solvent, followed by drying at 150℃ for 2 hrs and grounding was proposed. They achieved 92% removal of glyphosate at 15℃ with a maximum adsorption capacity of 46.8 mg/g [96].

Song *et al*. synthetized a GO-α-Fe_2O_3 nanocomposite by facile hydrolysis method and explored its properties as an additive for lubricating oil. After the addition of GO-α-Fe_2O_3 nanocomposite, the oil showed better friction and wear properties as GO nanosheets when combined with oil formed a thin tribal-film on the rubbing surface. Application of the same nanocomposite in solar energy conversion, environmental remediation, and advanced electric/optical devices was also suggested [84,88].

CHAPTER 3
METHODOLOGY

The objective thesis results in two major experimental parts:

1. Synthesizing of functionalized GO with metal: - GO-metal oxide composite.
2. Evaluating the capture capacity and phenomena of SO_2 on pristine GO and the functionalized GO.
3. Characterizing the GO and functionalized GO before and after the SO_2 capture.

Two different methods were used for the functionalization, to obtain nanoparticles of iron oxide deposited on GO, with different oxidation states and particle morphologies. The first method was using a polyol process with samples named GO-Fe_xO_y-P and the second method was and hydrothermal method with samples named GO-Fe_xO_y-H. The GO and iron oxide functionalized GO samples were tested for SO_2 capture under various operating conditions (temperature and low rates).

3.1 Experimental Procedure

3.1.1 Synthesis of material type 1 (GO-Fe_xO_y-P)

GO-Fe_xO_y-P samples were synthesized in two steps. Polyol method for the synthesis of Fe nanoparticles and wet deposition of Fe nanoparticles on the surface of GO. The polyol method involves the use of ethylene glycol as the main agent for the deposition of nanoparticles on the surface of the support. The quality of the nanoparticle is determined by the ratio of ethylene glycol and sodium hydroxide during the synthesis of nanoparticles [98]. The whole synthesis was used aiming to achieve the deposition of metallic iron nanoparticles on the surface of GO. GO-Fe_xO_y-P

is used to designate this type of sample unless the oxidation state is not confirmed. The concentration of added iron was targeted to be 5wt%.

3.1.1.1 Materials

Graphene oxide was purchased from ACS Materials. Iron nitrate nanohydrate ($FeNO_3.9H_2O$, precursor salt), ethylene glycol (99%), and sodium hydroxide (NaOH) pellets were bought from Fisher Scientific Canada.

3.1.1.2 Method

- Nanoparticle preparation: The precursor salt was mixed in a round bottom flask with ethylene glycol and a 0.12M solution of sodium hydroxide in ethylene glycol was added dropwise to maintain a pH of around 12 to control the size of the nanoparticles. The round bottom flask was then placed for quick reflux in a silicone oil bath at 160℃, thus completing the polyol process [98].
- Impregnation: A small amount of 2.63 mL of thus prepared Fe_xO_y nanoparticle refluxed solution was then mixed with GO (100 mg) and distilled water. The stirring was continued for a duration of 48 hrs to 72 hrs to ensure proper deposition of Fe nanoparticle on the surface of the support (GO), as more the time of stirring, the more uniform is the deposition of Fe nanoparticles on GO. After stirring, the solution was centrifuged, air-dried, and ground to obtain GO-Fe_xO_y-P powder. The method is summarized in Figure 3-1.

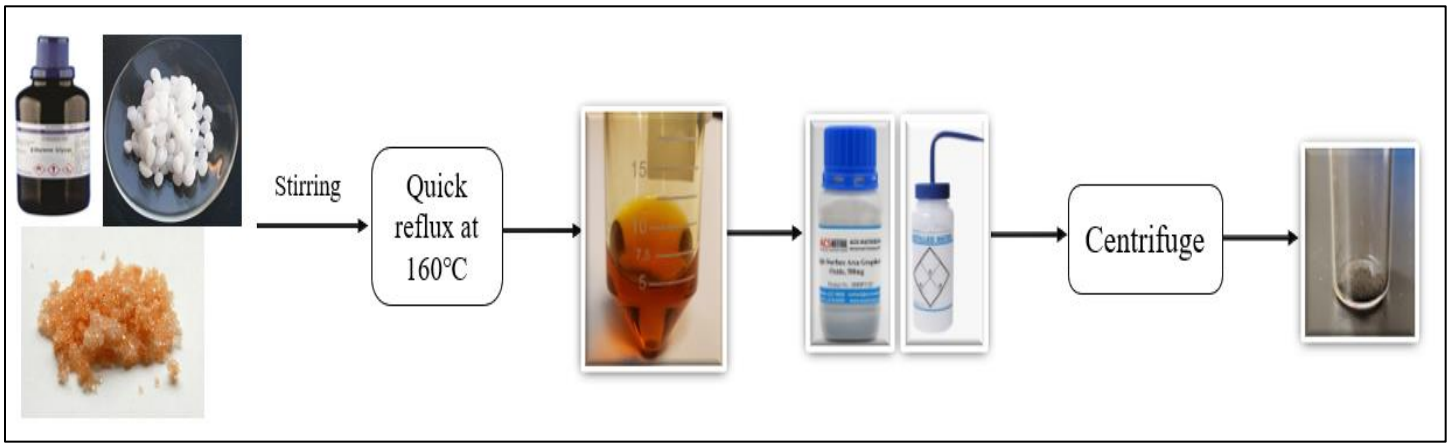

Figure 3-1: Schematic of wet deposition of Fe nanoparticles on GO using Polyol process.

3.1.2 Synthesis of material type 2 (GO-Fe_xO_y-H)

GO-FexOy-H was synthesized by the facile hydrolysis method [97]. The whole synthesis was used aiming to achieve the deposition of iron oxide nanoparticles on the surface of GO. GO-FexOy-H is used to designate this type of sample unless the oxidation state is not confirmed at this stage. The concentration of added iron was targeted to be 17w% at this stage for that methodology.

3.1.2.1 Materials

Iron chloride hexahydrate ($FeCl_3.6H_2O$, precursor salt) and ethanol were purchased from Fisher Scientific Canada and Graphene Oxide (GO) was bought from ACS Materials.

3.1.2.2 Method

The precursor salt was dissolved in 50 mL of distilled water in a round bottom flask and 50 mL of ethanol was added to it during continuous stirring on a magnetic stirrer. GO (50 mg) was then mixed and the solution was sonicated and then stirred for 30 mins. The homogenous solution thus obtained was then refluxed at 100°C for 2 hrs. After cooling,

the solution was centrifuged and then annealed in a furnace at 350℃ for 2 hrs. Thus, the obtained product was then ground to obtain GO-Fe_xO_y-H red powder. The method is summarized in Figure 3-2.

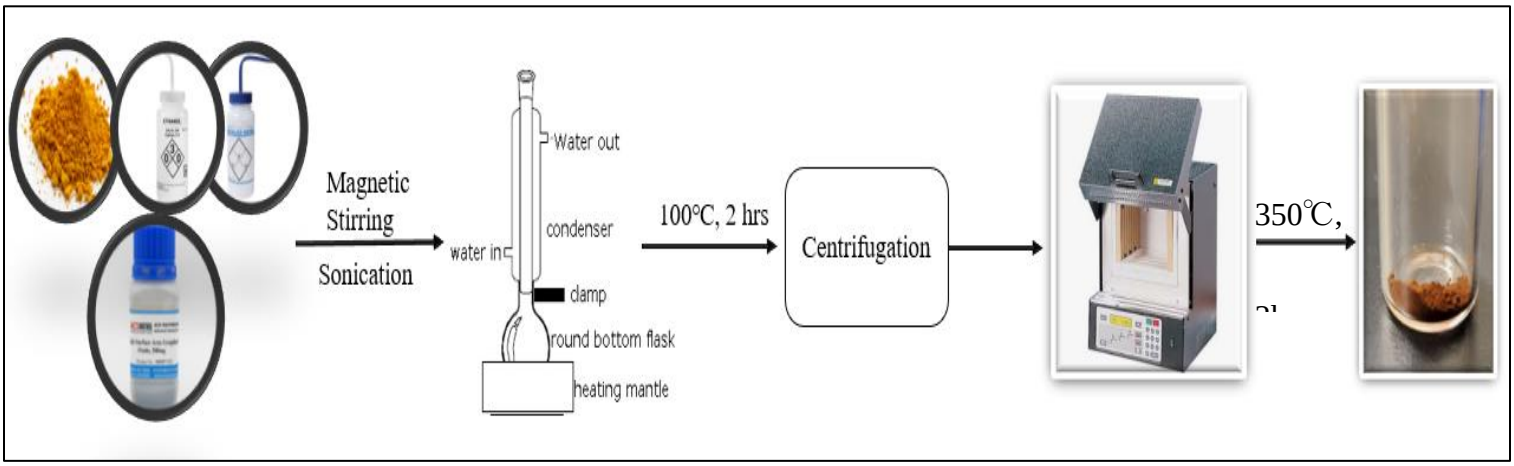

Figure 3-2 Schematic for hydrolysis method for iron oxide deposition on GO.

3.2 SO_2 capture experiments

3.2.1 Procedure for SO_2 capture and set-up

The setup of SO_2 capture using the materials had been designed as a PFR reactor, with a heating and cooling system, along with a detector (Draeger X-am 2500 detector) attached to the outlet.

As can be seen from Figure 3-3 the two gas cylinders, namely N_2 and SO_2 in Ar (35 ppm) were connected to their respective regulators and valves. The gas was then connected to the rotameter which controls the volumetric flow rate of the gas. Before the rotameter, a needle valve was placed which stabilizes the constant fluctuation in the readings by rotameter as it zeroes the influence of pressure change from the gas cylinders.

The rotameter was connected to the reactor system, which consisted of a 24 cm long and 0.25 mm in diameter quartz tube. The material for the capture of SO_2 was placed in the last quarter of the reactor so that the gas can get enough time to heat up to the desired temperature for the reaction. The sample bed itself had a length of about 1-2.5cm with a few cm of quartz wool placed before and after the sample (Figure 3-4).

The heating system consisted of a steel tube 20 cm long and 0.25 mm in diameter covering the quartz tube, to provide a heated environment for it, with heating tape wrapped securely around the steel tube to heat it. The insulation was provided in the form of two layers. One of insulation tape and another of the quartz wool and had been secured by the Kapton tape. A thermocouple was connected to the outlet end of the reactor and near the material (sandwiched between quartz wool) to measure the temperature in the vicinity of the material. The temperature was monitored by a temperature controller which was customed designed by the Science Electronics shop of uOttawa.

The outlet gas was cooled before entering the Draeger analyzer, as the detector cannot tolerate temperatures above 20°C. The cooling system is comprised of a steel tube 1 m long and 0.25 mm in diameter, a part shaped in form of a coil to provide more surface area for cooling of the gas. This coil-shaped tube was immersed in an ice bath and then connected to the detector.

The Draeger X-am 2500 detector measures only the concentration of SO_2 in ppm and is not calibrated to measure another gas concentration. The detector is isolated to reduce the influence of fumehood pressure. It is put in a plastic Ziploc-type bag and during the experiment, a vacuum is created inside it.

The whole setup, from the needle valve to the detector, was placed in the fume hood to avoid any danger which could have happened during the reaction.

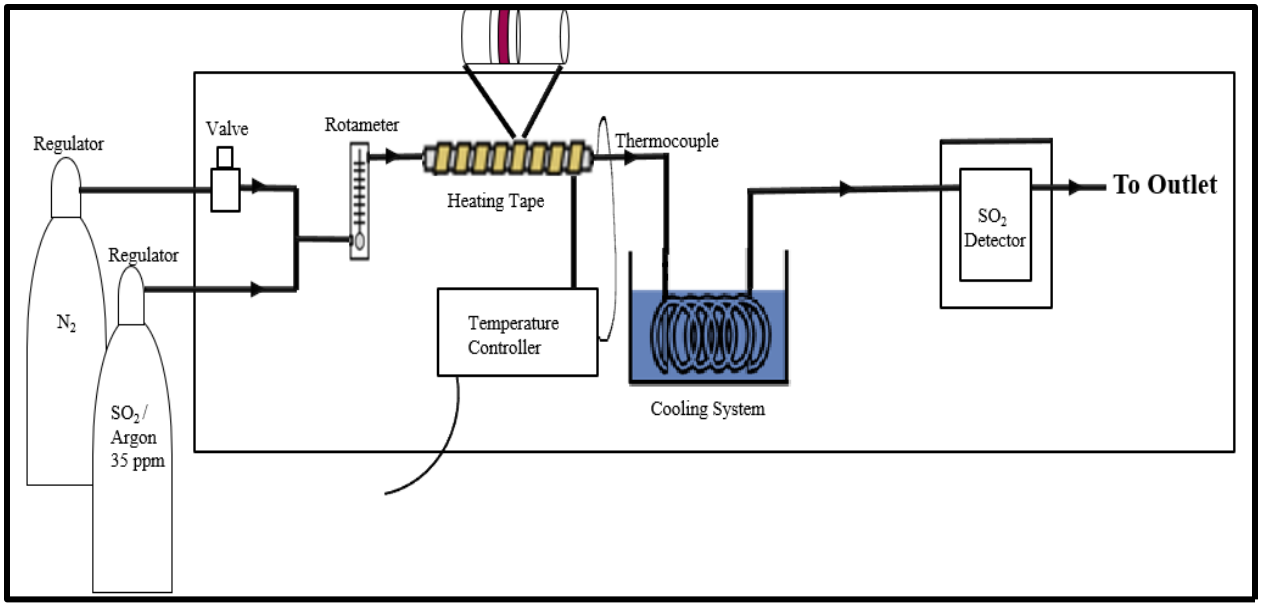

Figure 3-3: Schematic of SO_2 capture setup.

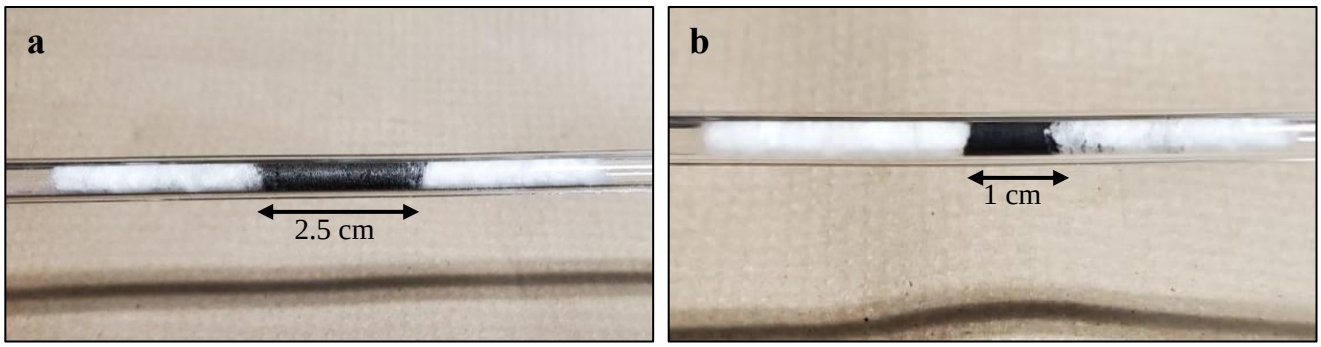

Figure 3-4: Quartz Tube containing 50 mg of sample sandwiched in between quartz wool, a. GO, and b. GO-Fe_xO_y-P.

The samples were pre-treated with N_2 gas within the system before the reactions, at room temperature, for the removal and desorption of any impurities present in the reaction system. The samples were not further pretreated by calcination or reduction before capture testing as GO is sensitive at high temperatures, thus the samples were used as it.

3.2.2 Design of Experiments (DOE)

The objective was to conduct the SO_2 capture experiments and analyze the behavior of the breakthrough curves across the chosen temperature and flowrate ranges for the various prepared material and pristine GO.

The lowest temperature was chosen to be room temperature (20℃) and 100℃ as the maximum. GO starts to decompose [99] rapidly at a temperature higher than 120℃ and loses the oxygen functionalities and water present on the surface, hence 100℃ was chosen as a maximum applicable temperature to be on the safe side. 60℃ was chosen as the center point.

The highest flowrate was chosen as 15 mL/min to ensure the stability of the material in the reactor. Since the saturation was achieved faster in some cases, the flow rate was varied from 5 mL/min to 15 mL/min with 10 mL/min as the center point. The information is summarized in Table 3-1.

Table 3-1: Chosen design factors and corresponding levels of full factorial design.

Factors/Levels	**Temperature (°C)**	**Flowrate (mL/min)**
-1	20	5
0	60	10
1	100	15

The focus for the SO_2 capture studies was on the GO and GO-Fe_xO_y-P prepared samples Thus, the DOE was applied to two different materials with a total of 12 runs, as shown in Table 3-2. A new sample was used for each experiment. The experiments were performed in random order.

Table 3-2: Full factorial design of SO_2 capture experiments with two different parameters.

Experimental Runs	Material	Temp	Flowrate
1	GO	-1	-1
2	GO	-1	1
3	GO	1	-1
4	GO	1	1
5	GO	0	0
6	GO	0	0
7	GO-Fe_xO_y-P	-1	-1
8	GO-Fe_xO_y-P	-1	1
9	GO-Fe_xO_y-P	1	-1
10	GO-Fe_xO_y-P	1	1
11	GO-Fe_xO_y-P	0	0
12	GO-Fe_xO_y-P	0	0

The GO-FexOy-H material was tested at 20 °C and 15 mL/min.

Before the experiments with the samples, blank runs were made at respective temperatures and flowrates. Even if the cylinder was initially calibrated to contains 35 ppm SO_2/Ar, the blank run curves showed the maximum attainable concentration at those conditions with an average 25 ppm. They were then used as the baseline for each set of the conditions and for comparisons among the materials and capacity calculations.

3.2.3 Capacity calculations

The capture capacity of the materials for SO_2 was calculated based on the following equation (3.1).

$$q = \frac{\left[\left(\int C_i - C_O\right)dt \times volumetric\ flowrate\right]}{Mass\ of\ material} \quad [3.1]$$

With the capacity (q) in g_{SO2}/g_{GO}, C_i the outlet concentration, C_o the inlet concentration, and t the time. A detailed description of the calculations is mentioned in Appendix 1. The flowrate of the reaction was varied from 5 mL/min to 15 mL/min and the mass of material was taken as 50 mg.

3.3 Material characterization

In this work, we have used SEM, TEM, and EDXS to study the surface morphology and elemental composition of the prepared samples.

The SEM was conducted by Zeiss Gemini SEM 500 in the Centre for Research and Photonics. The images were analyzed at three different magnifications and micron-scale. TEM was conducted by JEM-2100F FETEM (JEOL) in CaMAR and the sample analysis was done at different scales. The EDXS was conducted along with TEM, JEM-2100F FETEM (JEOL) in CaMAR.

CHAPTER 4
RESULTS AND DISCUSSIONS

This section presents the characterization of the samples – GO, GO-Fe_xO_y-P, and GO-Fe_xO_y-H– prior and after the SO_2 capture, and their respective capturing capacities. The fresh samples are analyzed using SEM, TEM, and EDXS analysis. The results for the capture and reaction of SO_2 with GO, GO-Fe_xO_y-P, and GO-Fe_xO_y-H are presented in the form of breakthrough curves and are compared accordingly, with a focus on the GO-Fe_xO_y-P and GO. The effect of SO_2 on the morphology and its interaction with the materials is demonstrated with TEM and EDXS analysis conducted after the reaction.

4.1 Characterization of fresh GO and functionalized GO

4.1.1 Morphology characterization using SEM

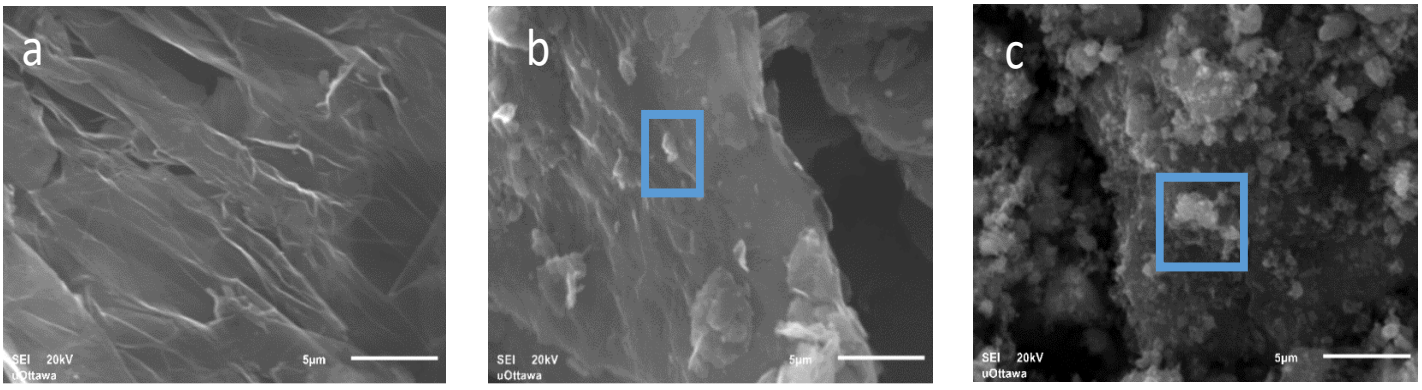

Figure 4-1: SEM images of a. GO; b. GO-Fe_xO_y-P; and c. GO-Fe_xO_y-H

Figure 4-1 shows the SEM image of pristine GO (Figure 4-1 a), GO-Fe_xO_y-P (Figure 4-1 b), and GO-Fe_xO_y-H (Figure 4-1 c) to analyze their surface morphology and the deposition of metal. Pristine GO is used for the capture of SO_2 and compared with the iron and iron oxide GO composites. The image confirms that the GO has a layered structure and that the sheets are stacked together to resemble a blanket, and the smooth edges are also visible clearly in Figure 4-6 a. These wrinkled sheets provide a large surface for SO_2 capture and metal deposition. Al-Gaashani *et al.* accounted for the wrinkles and folded regions of GO sheets for the sp^3 carbons and formation of oxygen-containing functional groups on the basal planes [1,14], hence providing possible oxidation sites to SO_2, as discussed in section 2.4.

The SEM image of GO shown in Figure 4-1a is used as a basis for comparison of GO with GO functionalized with iron and iron oxide. The morphology of the iron functionalized GO using the polyol process is resembling the pristine GO, with the addition of small islands noticed on the surface (Figure 4-1 b). These slight bumps can be a possible indication of the deposition of iron oxide on the surface but could not be directly associated with iron particles. Their diameters also range from 5µ to 2µ, which is larger than expected for the iron particles. The presence of iron has further been confirmed by EDXS analysis (see section 4.1.2). On the other hand, the GO morphology seems to have been conserved and layered structure can still be seen beneath the bumps.

On analyzing the GO-Fe_xO_y-H composite through SEM (Figure 4-1 c), it is seen that the changes in structure are more important. The numerous little grains observed on the surface are associated with the iron oxide particulates deposition, further analyzed by EDXS (see section 4.1.2). The amount of iron added was 3 times higher than for the GO-Fe_xO_y-P and therefore influenced the dispersion as well as GO / Fe_xO_y interaction. It can be observed that the addition of oxide of iron

using this method has caused aggregation of the layered structure of GO. One of the causes of aggregation can be the reduction of GO at high temperatures during drying as discussed by Song *et al* [100]. The behavior of GO-Fe_xO_y-H at high temperatures should be further confirmed by thermogravimetric analysis to clearly state the reason for aggregation – whether it is due to decomposition of GO or addition of Fe_xO_y – but the addition of Fe_xO_y seems one of the plausible reasons for aggregation. Due to aggregation, the surface area of the composite might have decreased which in turn might decrease the capture capacity of SO_2 (further discussed in section 4.2)

4.1.2 Surface composition analysis using EDXS

The elemental analysis was performed by EDXS to confirm the deposition of Fe, for both the composites, on the surface of GO. Figure 4-2 shows the EDXS of pristine GO (Figure 4-2 a), GO-Fe_xO_y-P (Figure 4-2 b), and GO-Fe_xO_y -H (Figure 4-3 c).

The analysis was performed on the specific regions indicated by points on the map, and not on the overall surface of the samples. Thus, the results of the analysis were focused more on those points, rather than the whole area of the sample.

Figure 4-2 a is used as the base to compare the addition of Fe on the surface of GO. The peak of Cu is because of using carbon and copper grid while performing the analysis. The TEM images of the samples used for EDXS are shown in the inset of the respective graphs, show the point at which the electron beam is focused and the same used to find the composition of the spectrum.

On comparing Figure 4-2 a with b, the addition of the Fe peak confirms the successful addition of Fe on the surface of GO. The EDXS analysis of GO-Fe_xO_y-H (Figure 4-2 c) shows the successful addition of Fe as well. There was a significant decrease in C/O peak heights ratios compare to the

GO and GO-Fe_xO_y-P, which could be an indication the iron might be in an oxidized state as aimed, but the relative concentration of Metal/GO is also influencing these ratios. In addition, the intensity of Fe and O height was height due to a larger iron deposition concentration. The particle sizes of deposited metal could not be determined using the TEM analysis.

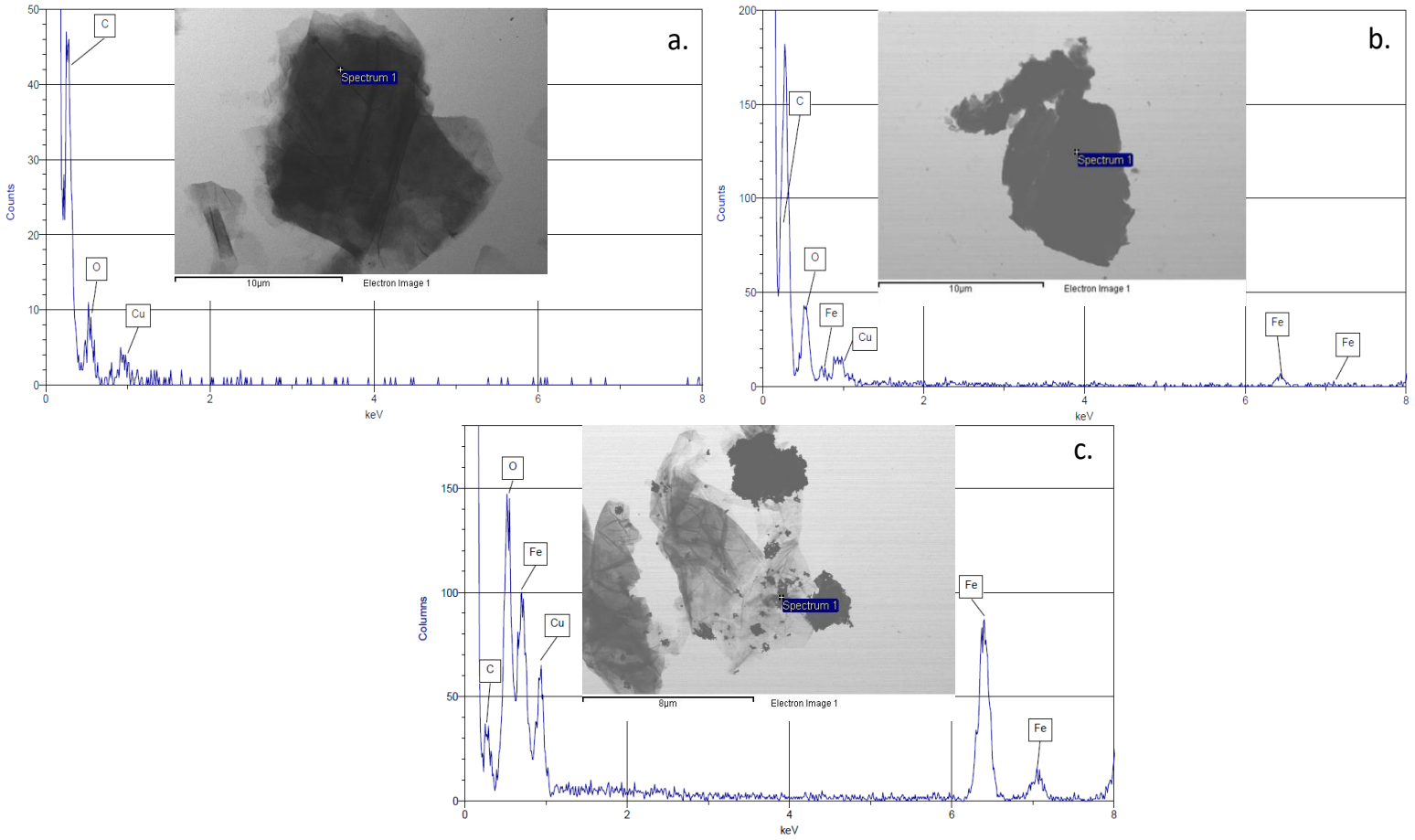

Figure 4-2 EDS analysis of a. GO; b. GO-Fe_xO_y-P and c. GO-Fe_xO_y-H

4.2 SO_2 capture studies

4.2.1 Breakthrough Curves and Capture Capacity

GO and GO-Fe_xO_y-P

The GO-Fe_xO_y-P and GO samples were thoroughly characterized for SO_2 capture, following DoE. The temperatures for DoE ranged from room temperature (20℃) to maximum temperature attainable with safety into consideration at 100℃ with a center point at 60℃. The rotameter flowrate varied from 5 mL/min (lowest) to 15 mL/min (highest) with a center point at 10 mL/min. The outlet concentration (ppm) from the detector was plotted against time (mins) at different temperatures and flowrates to obtain the breakthrough curves for each sample.

Breakthroughs are shown in Figure 4-3. Figure 4-3 a graph is for 20℃ and 5 mL/min, Figure 4-3 b for 100℃ and 5 mL/min, Figure 4-3 c for 60℃ and 10 mL/min, Figure 4-3 d graph is for 20℃ and 15 mL/min, and Figure 4-3 e graph is for 100℃ and 15 mL/min flowrate. For each set of conditions, a blank study was performed, giving information on the residence time, unsteady-state starting behaviour, and maximum concentration that can be measured. The maximum concentration was evaluated to be 25 ppm (slightly different than supplier-provided information). A blank experiment was performed for each set of operating conditions and used as the baseline.

In all figures, the typical breakthrough curve can be observed. For the blank runs, a steep change from the 0 to the maximum after a short delay is observed, coherent with the absence of sample. For GO and GO-Fe_xO_y-P, the change is less steep according to anticipated possible phenomena of capture and mass transfer limitations. The delay is generally longer for GO and then GO-Fe_xO_y-P, with less steep, and with longer time to reach saturation.

Figure 4-3 a. shows the breakthrough curves of GO and GO-Fe_xO_y-P at 20℃ temperature and 5 mL/min flowrate. First, the delay for the exit concentration was not observed for the GO-Fe_xO_y-P, which is most probably attributed to a delay in starting the acquisition. An analysis of the entire curve shows that the saturation was achieved at about 250 min for the GO and was not reached yet at 300 min for the GO-Fe_xO_y-P, readily indicating promising results. At the later stages of the curve, there is not much of a difference between the saturation concentration of blank and GO and they both have merged towards the end. The GO curve starts saturating around 150 mins (around 2 hrs into the reaction). Whereas, for GO-Fe_xO_y-P, the saturation starts around the same time (150 mins) and it continues even after 300 mins (5 hrs) with the concentration nears 20 ppm and maximum outlet concentration not yet reached.

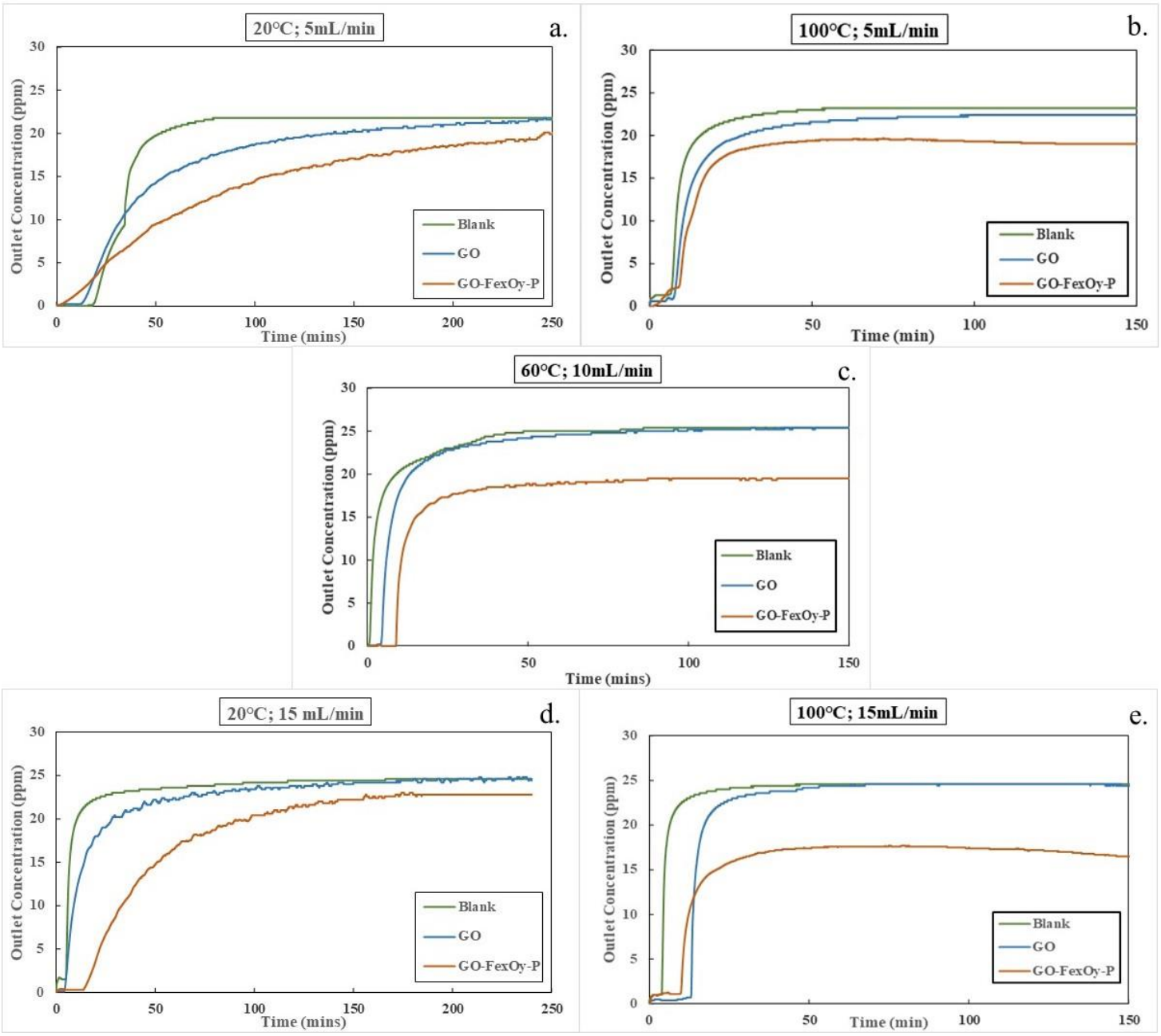

Figure 4-3: Breakthrough curves at a. 20°C and 5 mL/min; b. 100°C and 5 mL/min; c. 60°C and 10 mL/min; d. 20°C and 15 mL/min and e. 100°C and 15 mL/min.

On focusing on the higher temperature (100°C) graph Figure 4-3 b, the graph trend changes a bit but without significant differences. The breakthrough time for GO slightly increases to around 15

mins and for GO-Fe_xO_y-P, it slightly increases. The GO-Fe_xO_y-P curve tends to follow a gradual increase first and then it starts increment speedily. Whereas GO curve even though shows a better performance than the low temperature one, still starts its saturation in just 25 mins into the reaction and GO-Fe_xO_y-P follows the same.

On focusing on the latter part of the graph, both GO and GO-Fe_xO_y-P reached a steady-state. While GO reached full saturation, GO-Fe_xO_y-P was stable at around 18 ppm. Hence, the addition of Fe on GO has increased the capturing capacity at both low (20℃) and high (100℃) temperatures at low flowrate.

Figure 4-3 c. shows the breakthrough curves of GO and GO-Fe_xO_y-P at 60℃ and 10 mL/min. The pattern of both breakthrough curves seems to be similar. The breakthrough time has increased to around 10 mins for GO-Fe_xO_y-P from less than 5 mins for GO, indicating that the higher capacity. The time to become saturated increased, thereby further increasing the capturing capacity of SO_2 for the material.

On taking a glance at the later part of the graph and comparing them with the blank run, there is no significant difference between the saturation concentration of blank and the GO and they both have merged towards the end. The GO curve starts saturating before 25 mins (way less than 1 hr) and is saturated after 50 mins (1 hr into the reaction) with the concentration of approx. 25 ppm. Whereas, for GO-Fe_xO_y-P, the saturation starts around the same time (25 mins) and it reaches an almost steady-state after 50 mins (less than an hour into the reaction) with a concentration of around 18 ppm lower than the maximum. Hence, the performance of GO-Fe_xO_y-P is better than that of GO for SO_2 capture even at a medium temperature and more than for the lower temperature as explained previously.

Figure 4-3 d and e show the breakthrough curve of GO and GO-Fe_xO_y-P when reacted with SO_2, at 20℃ and 100℃ respectively for a flow rate of 15mL/min.

On looking at the breakthrough curves of Figure 4-3 d (20℃), the change in the trend of the breakthrough curve from GO to GO-Fe_xO_y-P can be distinctly seen. The breakthrough time has increased to around 20 mins for GO-Fe_xO_y-P from less than 5 mins for GO. Thus, this means that a longer time is taken by GO-Fe_xO_y-P to capture SO_2 and become saturated. This further increases the capturing capacity of SO_2 for the material. The increase in capacity related to an increase in flow rate is indicating of mass transfer limitations phenomena (further discussed in the later section).

On taking a glance at the later part of the graph and comparing them with the blank run, there is no significant difference between the steady-state concentration of the blank and GO, indicating GO reaches saturation. The GO curve starts saturating before 50 mins (less than 1 hr) and is saturated around 150 mins (1 hr and 20 mins into the reaction) with a concentration of approx. 25 ppm. Whereas, for GO-Fe_xO_y-P, the saturation starts around 140 mins (2 hrs and 20 mins) and is almost saturated after 180 mins (3 hrs into the reaction). Hence, at low temperatures, the additional performance of GO-Fe_xO_y-P is better than that of GO for SO_2 capture at all flow rates.

On focusing on the higher temperature (100℃) graph Figure 4-3 e, the graph trend changes a bit. The breakthrough time for GO slightly increases to around 13 mins when compared with GO-Fe_xO_y-P whose decreases to 10 mins. Hence, at a higher temperature, the breakthrough time has decreased slightly for GO-Fe_xO_y-P and GO will take a bit more time to saturate.

But when we narrow down to the later part of the graph, we can see that the saturation for both GO and GO-Fe_xO_y-P starts around the same time 25 mins for GO and around 30 mins for GO-

Fe_xO_y-P, but the saturation is reached for GO (same as for 20℃) as it is not for the GO-Fe_xO_y-P. GO-Fe_xO_y-P reached a steady-state around 16 ppm. On comparing both the materials with blank run the saturation concentration of GO is reached as it is equal to blank but for GO-Fe_xO_y-P it stabilizes at a value which is approximately 9 ppm less than blank. This could be indicating reaction phenomena happening and GO-Fe_xO_y-P acting as a catalyst rather than just a sorbent and reaching an equilibrium point. It would have to be confirmed if there is a conversion into SO_3, and if such produced species are then adsorbed or emitted.

The decrease in performance of GO at high temperatures can be because of the decomposition of GO as the temperature increases. This can be attributed to the loss of water molecules as the temperature is increased. Chang *et al.* conducted TG analysis of GO and concluded that within the temperature range of 40-110℃ there is a 12.09% of weight loss as the degradation of GO starts and it is due to loss of the water molecules [101]. These water molecules provide hydrogen bonding within the different layers of GO, providing reaction sites for SO_2.

Thus, we can conclude that at the higher temperature (as for at lower temperature) the GO-Fe_xO_y-P is performing better than GO for the capture of SO_2. Also, on comparing both d and e. the addition of Fe on GO has increased the capture capacity for both the temperatures and at high temperatures, GO-Fe_xO_y-P is performing better.

The breakthrough time gradually increases with an increase in temperature and flowrate as demonstrated by Figure 4-3, implying a better capture capacity as the materials are taking longer to get saturated. In addition, a lower steady-state concentration was reached for the GO-Fe_xO_y-P at higher temperatures, as mentioned above.

Figure 4-4 a. shows the capture capacities calculated for GO and GO-Fe_xO_y-P at 20℃ and 100 ℃ at 15 mL/min, and Figure 4-4 b. for GO and GO-Fe_xO_y-P at 20℃, 60 ℃ and 100 ℃ at 5 mL/min and 10 mL/min. At the same flowrate but at different temperatures, Figure 4-4 a, the capture capacity of GO is almost the same but the increase in the temperature has worked in the favor of GO-Fe_xO_y-P and as increasing the capture capacity, coherent with capturing phenomena other than just physisorption. These capacities are calculating considering that the SO_2 not going out from the system measured by the detector correspond to the SO_2 captured and converted.

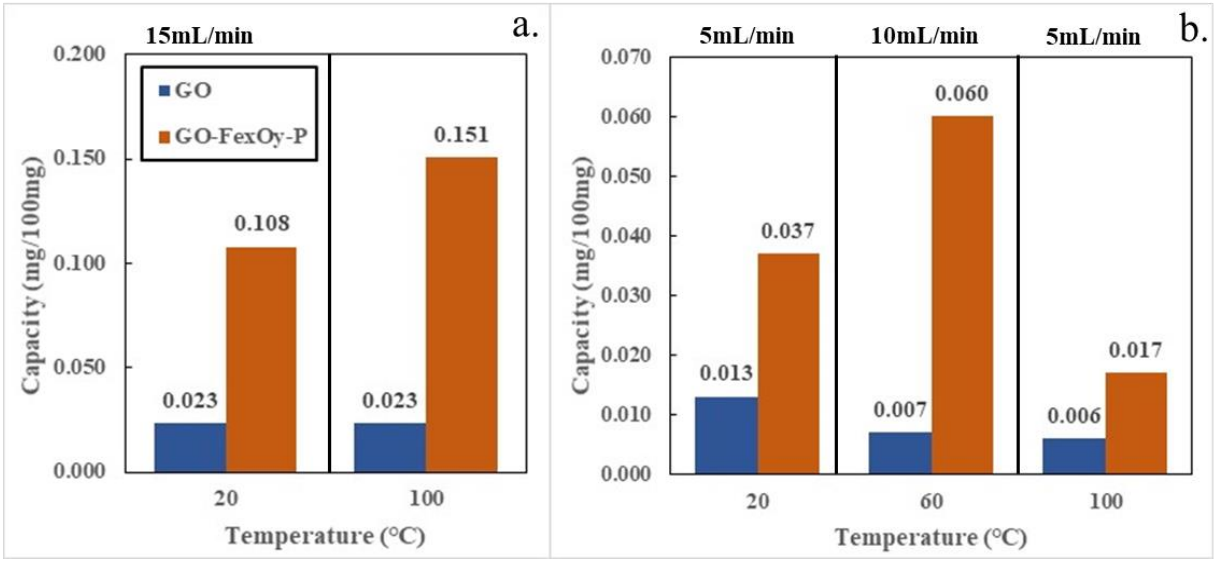

Figure 4-4: Calculated capture capacity of SO_2 using GO and GO-Fe_xO_y-P at a. 15 mL/min flowrate and reaction temperature as 20℃ and 100℃ and b. 5 mL/min and 10 mL/min flowrate and reaction temperature as 20℃,60℃ and 100℃.

As the flowrate is increased from 5 mL/min to 15 mL/min, Figure 4-4b, at the same temperature, 20℃, the capture capacity has decreased for GO and GO-Fe_xO_yP considerably. At the same flowrate and higher temperature, 15 mL/min and 100℃, the capture capacity has dropped for both GO and GO-Fe_xO_y-P. For the 10 mL/min and 60℃, the capture capacity is better than its counterparts in the same Figure 4-4 b.

Thus, we can see that with an increase in temperature and flowrate, together, the capture capacity has increased by almost by an order of 1 magnitude. The rise in the capacity with flowrate indicates the possibility of the reaction being external diffusion-related. The change in temperature at 15 ml/min can also be related to surface reaction, as the kinetic rate will increase with temperature, in opposition to pure adsorption that would decrease with an increase in temperature. The supplemental analysis is needed to understand and confirm the major phenomenon behind the capture process at various temperatures. The main conclusion is that the GO could capture SO_2 to some extent and that the addition of iron increases significantly the capture capacity, according to the thesis hypothesis.

GO-Fe_xO_y-H

Figure 4-5 shows the breakthrough curve of GO, GO-Fe_xO_y-P, and GO-Fe_xO_y-H at 20℃ and 15 mL/min. GO-Fe_xO_y-H led to less conclusive results for SO_2 capture, but are shown for comparison and importance of parameters such as the amount of metal added and the oxidation state for further studies. The breakthrough time for GO-Fe_xO_y-H is the earliest when compared with GO and GO-Fe_xO_y-P, around 5 mins into the reaction and similar to the blank. The trend of the GO-Fe_xO_y-H curve is in fact similar to that of the blank curve. It starts rising and reached a steady state around 10 mins after the reaction start and achieves a steady-state around 25 mins into the reaction, with a steep increase. But on glancing at the later part of the graph, GO-Fe_xO_y-H steady-state

concentration is lower than that of GO and approximately equal to that of GO-Fe_xO_y-P, at 22.8 ppm which is a slight difference for which the significance still has to be confirmed.

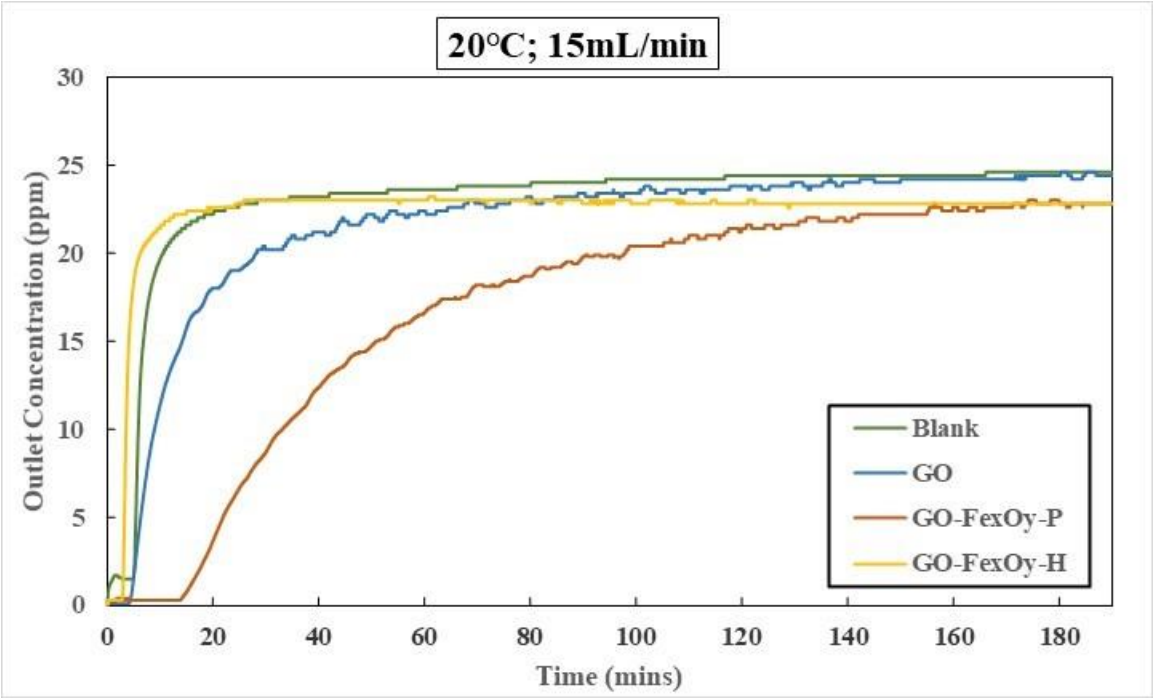

Figure 4-5: Breakthrough curves for GO, GO-Fe_xO_y-P, and GO-Fe_xO_y-H at 20°C and 15 mL/min.

The capturing capacity of GO-Fe_xO_y-H was calculated as 0.019 mg/100mg of GO, at 20°C and 15mL/min, which is slightly lower than GO and significantly lower than the GO-Fe_xO_y-P at the same temperature and flowrate. Thus, the performance of GO-Fe_xO_y-H is overall not good for SO_2 capture which can be related to the possible difference in the oxidation state of the Fe, but also the fact that the GO surface was mostly covered by the Fe deposited, preventing its participation in the capture process. The amount of metal deposited, and its oxidation state is, therefore, an

important parameter to look at. Moreover, more reactions at different temperatures and flowrate could be performed to properly conclude the performance of GO-Fe_xO_y-H as a material for the capture of SO_2.

4.2.2 Morphology characterization using TEM and surface composition analysis with EDXS

To have a look at the changes in the morphology after the reaction with SO_2, TEM analysis was conducted. When compared the before and after images of GO, GO-Fe_xO_y-P, and GO-Fe_xO_y-H from Figure 4-5, the change can be described as the addition of the black spots after the reaction.

Figure 4-5 a. shows the TEM image of GO before SO_2 capture. The layered structure of GO is visible. The thin paper-like structure of GO provides a high surface area, in turn providing reaction sites for the SO_2 and facilitates the reaction as well as being surface for metal deposition. After the reaction of GO with SO_2, Figure 4-5 b, shows black spots coagulated on the surface of GO which could be indicating sulfur adsorbed on the surface They seem like black ink spots on the paper-like structure of GO. The distribution of these spots is non-uniform, signifying that the SO_2 was probably not uniformly captured by the surface.

Figure 4-5 c is the TEM image of GO-Fe_xO_y-P before capture. Though the edges have seemed to be a bit darkened, the layered structure of GO has been maintained after the addition of Fe, hereby confirming the results from SEM analysis (Figure 4-1 b). After the reaction with SO_2 (Figure 4-5 d), the black ink type appearance spots are visible, similar to that in Figure 4-5 b. The distribution of the black area is not uniform again suggesting random capture of SO_2. Also, there is no conclusive evidence of the shape and size of the Fe particles, thus a more focused analysis, HRTEM, needs to be performed for further study.

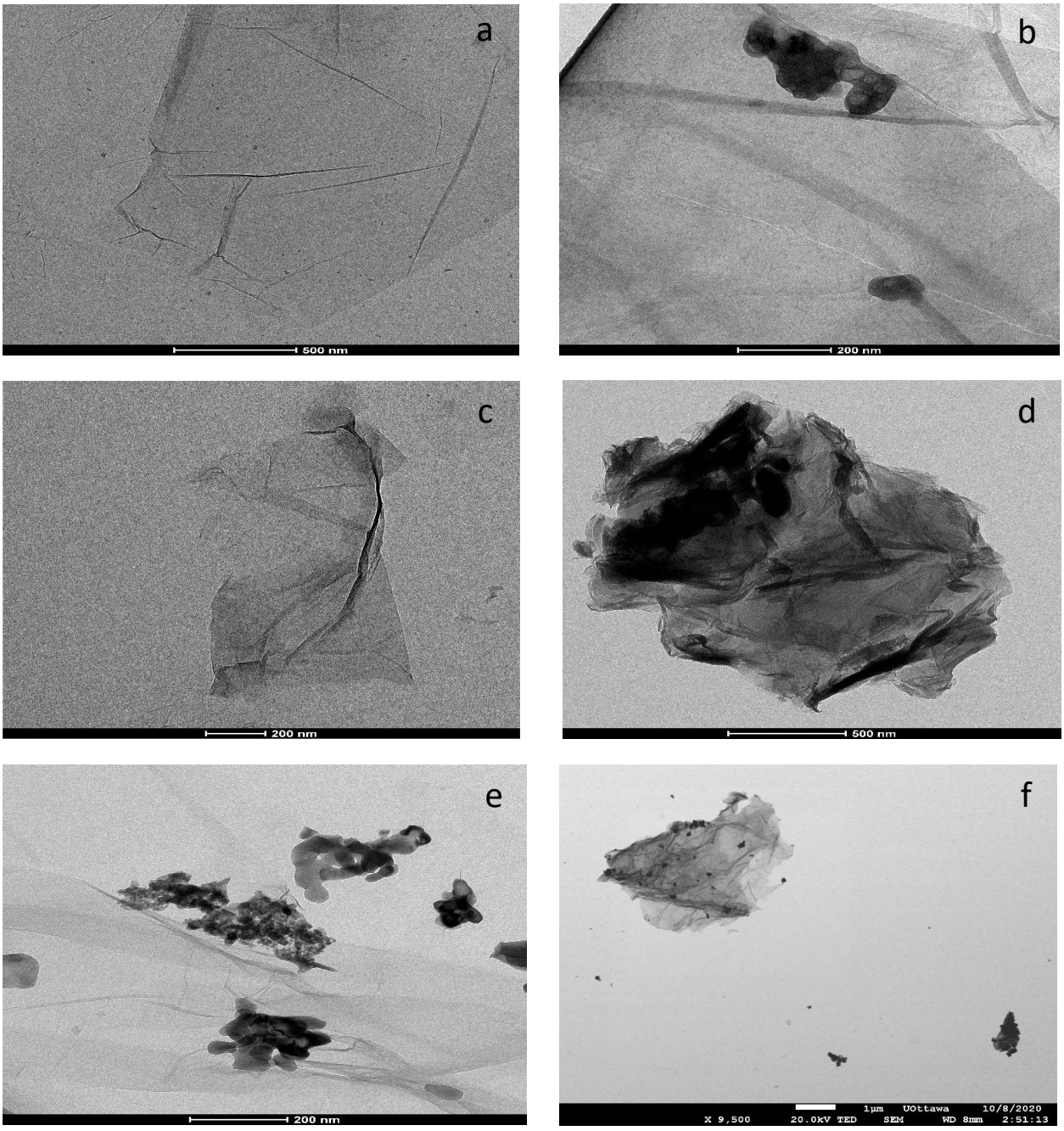

Figure 4-6: TEM analysis images of a. GO; b. GO-S; c. GO-Fe_xO_y-P; d. GO-Fe_xO_y-P-S; e. GO-Fe_xO_y-H and f. GO-Fe_xO_y-H -S.

The TEM image of GO-Fe_xO_y-H is shown in Figure 4-5 e. The base or the support seems to be layered at certain points but crumbled at others. The dark spots present at certain parts of the surface seem to have disturbed the layered structure of GO and have seemed to be in the form of aggregates. Also, these aggregates seemed to have been irregularly distributed on the surface of GO. After the reaction with SO_2, Figure 4-5 f. the dark spots on the surface are visible and are larger than for the two other types (GO and GO-Fe_xO_y-P). The SEM image shows the uneven arrangement of the dark spots suggesting a non-uniform SO_2 capture.

All dark spots were further analyzed by EDXS and the analyzed spectrum is shown in the inset of the EDXS graph analysis in Figure 4-6. The EDXS analysis results show the presence of S on the surface of reacted GO. Thus, we can conclude that GO indeed captured sulfur, but the speciation or oxidation state is unknown. When the spectrum area was changed from dark to light spots, the intensity of the sulfur peak decreased indicating that the sulfur is concentrated in the dark spot as expected from the TEM image and is not uniformly adsorb by the GO.

For the GO-Fe_xO_y-P, the blackened area analysis by EDXS confirmed the presence of sulfur after reaction with SO_2 on the surface. On varying the positions for the spectrum, from dark to light, the intensity of the sulfur peak varied as for the GO. It confirms that the GO-Fe_xO_y-P not just catalyzed a reaction from SO_2 to another compound but also captured the sulfur.

Thus, the capture of SO_2 by GO and GO-Fe_xO_y-P was analyzed by TEM and EDXS characterization techniques following capture studies and results are coherent with the breakthrough curves and capacities at various temperatures and flowrates. Overall, GO-Fe_xO_y-P

captured more sulfur and is confirmed by EDXS, though the state of sulfur is yet to be analyzed by an in-situ analysis of the whole reaction.

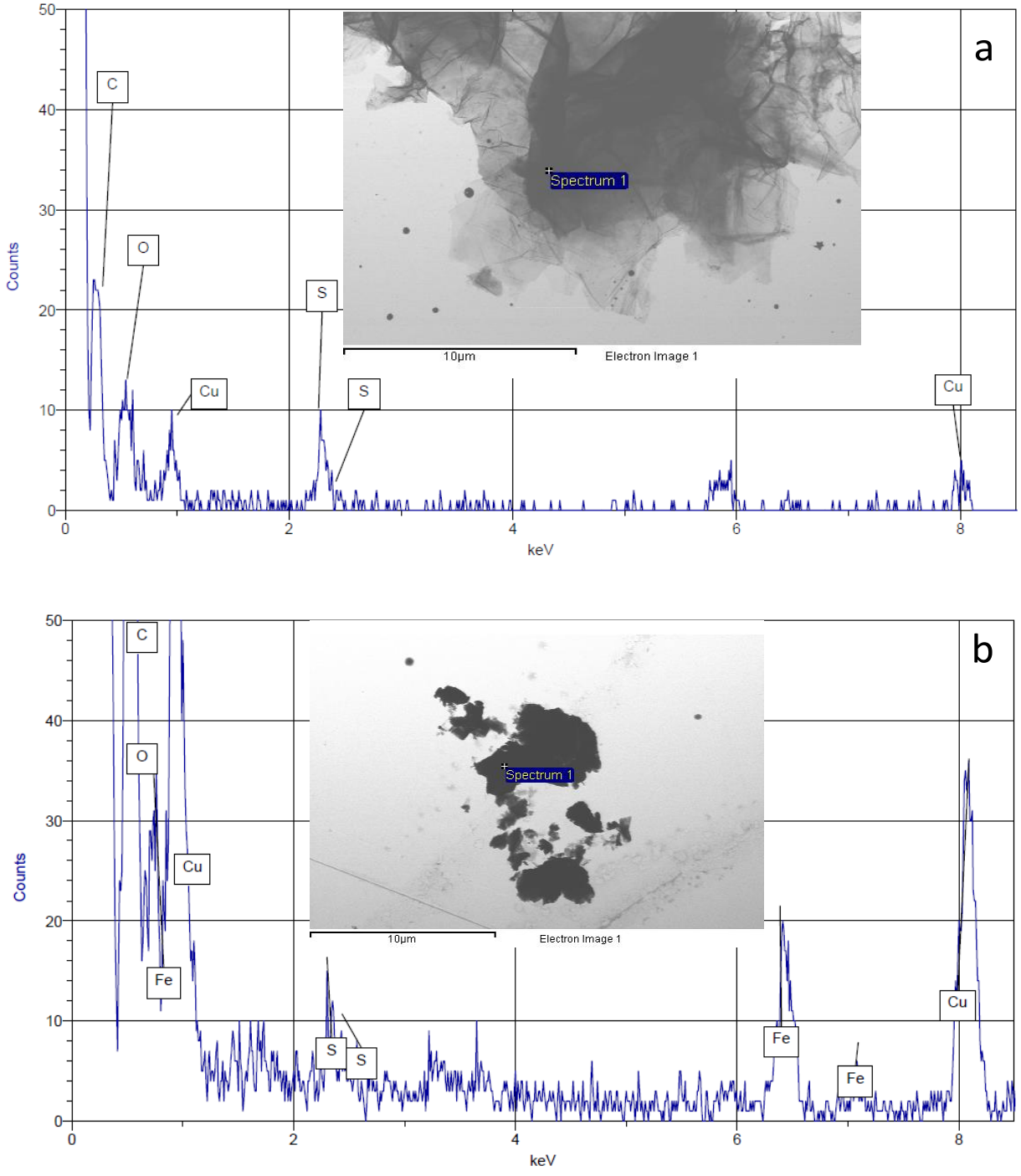

Figure 4-7: EDXS analysis of a. GO-S and b. GO-Fe_xO_y-P-S.

CHAPTER 5
CONCLUSIONS

To capture SO_2 at relatively low temperatures, GO was functionalized with iron to evaluate if the capacity can be enhanced by a combination of the phenomena. We were able to synthesize GO-based composites, by polyol process followed by wet deposition for GO-Fe_xO_y-P and hydrolysis process for the GO-Fe_xO_y-H. Characterization of the prepared samples was conducted by SEM, TEM, and EDXS, where the deposition of Fe was confirmed along with morphological changes.

The capture of SO_2 was achieved by thus synthesized materials and the breakthrough curves obtained show the difference in the efficiency of the prepared samples. On the calculation of the capture capacity, it was found that it considerably increased with the addition of Fe_xO_y on GO, being up to 4 times the on of only GO. It also increased with temperature and flowrate. The influence of the flowrate suggests that it is external diffusion-limited. At a higher flow rate, the influence of the temperature is coherent with the mass transfer limitation, but also with a surface reaction with a rate increasing with temperature. This phenomenon was however not observed at 5 ml/min, where the capacities are however much lower. The changes in morphology after the reaction were observed by TEM analysis and the presence of sulfur on the reacted samples was confirmed. Finally, the GO-Fe_xO_y-H samples showed significantly lower performance for SO_2 capture but indicated that the oxidation state and/or metal quantity might be important parameters, as expected.

Samples have been characterized and useful information was obtained but also opened to other research questions. Though the oxidation state, size, and the distribution of Fe_xO_y particles must

be confirmed using other methods such as XPS or XRD analysis as well as high-resolution TEM. Further characterization studies such as surface area by N_2 adsorption (BET), and TGA would be useful to get a better insight into the material characteristics. Main information to clarify are the oxidation state as well as the shape and size of the nanoparticles.

In addition, only the SO_2 was monitored at the outlet of the system. It would be important to confirm there is no SO_3 or other species going out. In situ studies will also permit us to get a better understanding of the mechanism and phenomena during the capture. These additional characterizations could conduct to the improvement of the preparation methods and synthesized materials.

In the objective of having an application process, the regeneration of the samples, the effect of various pre-treatment, and the limits of operating conditions, must be evaluated. For the regeneration, considering that the sulfur is probably not only physisorbed, parameters and treatment would have to be optimized for efficient regeneration. As for the operating parameters, an important one is temperature as it could directly impact the stability of the material. In addition, other metals could be tested to evaluate their performance. Finally, even though the samples present a reasonable capture capacity at room temperature, we still need to perform the experiments on a large scale to know the behavior of high-volume gas and do thorough cost-analysis.

References

[1] D. J. Babu *et al.*, “SO 2 gas adsorption on carbon nanomaterials : a comparative study,” pp. 1782–1792, 2018.

[2] Graham Readfearn, “Giant Antarctic iceberg on collision course with British territory of South Georgia.”

[3] F. Rezaei, A. A. Rownaghi, S. Monjezi, R. P. Lively, and C. W. Jones, “SO<inf>x</inf>/NO<inf>x</inf> Removal from Flue Gas Streams by Solid Adsorbents: A Review of Current Challenges and Future Directions,” *Energy and Fuels*, vol. 29, no. 9, pp. 5467–5486, 2015.

[4] C. C. for O. H. & Safety, “What are the potential health effects of sulfur dioxide?” [Online]. Available: https://www.ccohs.ca/oshanswers/chemicals/chem_profiles/sulfurdi.html.

[5] C. O. N. RESOURCES, N. A. O. SCIENCES, N. A. O. ENGINEERING, and N. R. COUNCIL, “Air Quality and Stationary Source Emission Control, Chapter: 10 Some Methods of Reducing Sulfur Oxides from Power Plants.”

[6] S. Ahirwar *et al.*, “Sulfur Dioxide Capture by Heterogeneous Oxidation on Hydroxylated Manganese Dioxide,” *ACS Omega*, vol. 38, no. 11, pp. 4970–4974, 2017.

[7] J. Nava, “PROVEN METHODS FOR REDUCING SULFUR DIOXIDE (SO2) EMISSIONS.”

[8] I. Ali, Z. A. ALOthman, and A. Al-Warthan, “Sorption, kinetics and thermodynamics studies of atrazine herbicide removal from water using iron nano-composite material,” *Int. J. Environ. Sci. Technol.*, vol. 13, no. 2, pp. 733–742, 2016.

[9] T. Y. K. and S. H. LEE, “Combustion and Emission Characteristics of Wood Pyrolysis Oil-Butanol Blended Fuels in a Di Diesel Engine,” *Int. J. …*, vol. 13, no. 2, pp. 293–300, 2012.

[10] A. Poullikkas, “Review of Design, Operating, and Financial Considerations in Flue Gas Desulfurization Systems,” *Energy Technol. Policy*, vol. 2, no. 1, pp. 92–103, 2015.

[11] A. Azetsu, H. Koga, A. Isogai, and T. Kitaoka, “Synthesis and Catalytic Features of Hybrid Metal Nanoparticles Supported on Cellulose Nanofibers,” pp. 83–96, 2011.

[12] “Catalysis Today, 10 (1991) 67-71,” vol. 10, pp. 67–71, 1991.

[13] F. Li, X. Jiang, J. Zhao, and S. Zhang, “Graphene oxide : A promising nanomaterial for energy and environmental applications,” *Nano Energy*, vol. 16, pp. 488–515, 2015.

[14] D. R. Dreyer, S. Park, W. Bielawski, and R. S. Ruoff, “The chemistry of graphene oxide,” 2010.

[15] S. Wan, W. Ding, Y. Wang, J. Wu, Y. Gu, and F. He, “Manganese oxide nanoparticles impregnated graphene oxide aggregates for cadmium and copper remediation,” *Chem. Eng. J.*, vol. 350, no. June, pp. 1135–1143, 2018.

[16] Y. Lei, F. Chen, Y. Luo, and L. Zhang, "Three-dimensional magnetic graphene oxide foam/Fe3O4 nanocomposite as an efficient absorbent for Cr(VI) removal," *J. Mater. Sci.*, vol. 49, no. 12, pp. 4236–4245, 2014.

[17] R. K. Srivastava and W. Jozewicz, "Flue gas desulfurization: The state of the art," *J. Air Waste Manag. Assoc.*, vol. 51, no. 12, pp. 1676–1688, 2001.

[18] P. B. C. Forbes and R. M. Garland, *Outdoor Air Pollution*, vol. 73. Elsevier Ltd, 2016.

[19] S. Biswas, "Wake up! See how pollution is eating away our monuments," pp. 1–15, 2017.

[20] W. Xie, L. T. Weng, C. K. Chan, K. L. Yeung, and C. M. Chan, "Reactions of SO2 and NH3 with epoxy groups on the surface of graphite oxide powder," *Phys. Chem. Chem. Phys.*, vol. 20, no. 9, pp. 6431–6439, 2018.

[21] S. J. Smith, J. Van Aardenne, Z. Klimont, R. J. Andres, A. Volke, and S. Delgado Arias, "Anthropogenic sulfur dioxide emissions: 1850-2005," *Atmos. Chem. Phys.*, vol. 11, no. 3, pp. 1101–1116, 2011.

[22] ECCC, "Acid rain: causes and effects." [Online]. Available: https://www.canada.ca/en/environment-climate-change/services/air-pollution/issues/acid-rain-causes-effects.html.

[23] M. Hopkin, "Acid rain still hurting Canada."

[24] ECCC, "Reducing acid rain." [Online]. Available: https://www.canada.ca/en/environment-climate-change/services/air-pollution/issues/acid-rain-causes-effects/reducing.html.

[25] ECCC, "Canada's response." [Online]. Available: https://www.canada.ca/en/environment-climate-change/services/air-pollution/issues/acid-rain-causes-effects/reducing.html.

[26] M. A. Hanif, N. Ibrahim, and A. Abdul Jalil, "Sulfur dioxide removal: An overview of regenerative flue gas desulfurization and factors affecting desulfurization capacity and sorbent regeneration," *Environ. Sci. Pollut. Res.*, 2020.

[27] Environment and Climate Change Canada, *Canada's Air Pollutant Emissions Inventory Report: executive summary - Canada.ca*. 2019.

[28] ECCC, "Calculating the total reduced sulphur threshold." [Online]. Available: https://www.canada.ca/en/environment-climate-change/services/national-pollutant-release-inventory/report/sector-specific-tools-calculate-emissions/total-reduced-sulphur.html.

[29] P. Bajpai, "Environmental Issues and Challenges," *Pulp Pap. Ind.*, pp. 221–230, 2017.

[30] R. Mckitrick and E. Aliakbari, "An Environmental Success Story," no. April, 2017.

[31] ECCC, "Air pollutant emissions." [Online]. Available: https://www.canada.ca/en/environment-climate-change/services/environmental-indicators/air-pollutant-emissions.html.

[32] A. A. Abdulrasheed, A. A. Jalil, S. Triwahyono, M. A. A. Zaini, Y. Gambo, and M. Ibrahim, "Surface modification of activated carbon for adsorption of SO2 and NOX: A review of

existing and emerging technologies," *Renew. Sustain. Energy Rev.*, vol. 94, no. X, pp. 1067–1085, 2018.

[33] "Journal of the Air Pollution Control Association A History Of Flue Gas Desulfurization Systems Since 1850," 2012.

[34] I. Mochida *et al.*, "Removal of SO< sub> x</sub> and NO< i> x</i> over activated carbon fibers," *Carbon N. Y.*, vol. 38, no. 2, pp. 227–239, 2000.

[35] M. M. Meimand and N. Javid, "Adsorption of Sulfur Dioxide on Clinoptilolite / Nano Iron Oxide and Natural Clinoptilolite," vol. 8, no. 2, 2019.

[36] G. E. World, "Flue Gas Desulfurization (FGD) System Market Worth 21.00 Bn USD by 2022."

[37] A. Miszczyk and K. Darowicki, "Reliability of Flue Gas Desulphurisation Installations - The Essential Condition of Efficient Air Pollution Control," *Polish J. Environ. Stud.*, vol. 11, no. 3, pp. 205–209, 2002.

[38] Y. Sun, E. Zwolińska, and A. G. Chmielewski, "Technology Abatement technologies for high concentrations of NO x and SO 2 removal from exhaust gases : A review," *Crit. Rev. Environ. Sci. Technol.*, vol. 46, no. 2, pp. 119–142, 2016.

[39] P. S. Wheatley *et al.*, "NO-releasing zeolites and their antithrombotic properties," *J. Am. Chem. Soc.*, vol. 128, no. 2, pp. 502–509, 2006.

[40] A. Srinivasan and M. W. Grutzeck, "The adsorption of SO2 by zeolites synthesized from fly ash," *Environ. Sci. Technol.*, vol. 33, no. 9, pp. 1464–1469, 1999.

[41] S. Kocabas, "Adsorption equilibrium and breakthrough analysis for sulfur dioxide adsorption on silica gel," vol. 41, pp. 223–230, 2002.

[42] B. Y. S. Chang *et al.*, "Progress in the functional modification of graphene/graphene oxide: A review," *RSC Adv.*, vol. 10, no. 1, pp. 15328–15345, 2017.

[43] B. E. Alver, M. Sakizci, and E. Yörükoğullari, "Adsorption of Sulphur Dioxide Using Natural and Modified Gördes Clinoptilolites," *Adsorpt. Sci. Technol.*, vol. 29, no. 4, pp. 413–422, May 2011.

[44] Nanoshell, "METAL ORGANIC FRAMEWORKS." [Online]. Available: https://www.nanoshel.com/metal-organic-frameworks.

[45] M. Savage *et al.*, "Selective Adsorption of Sulfur Dioxide in a Robust Metal–Organic Framework Material," *Adv. Mater.*, vol. 28, no. 39, pp. 8705–8711, 2016.

[46] G. L. Smith *et al.*, "Reversible coordinative binding and separation of sulfur dioxide in a robust metal–organic framework with open copper sites," *Nat. Mater.*, vol. 18, no. 12, pp. 1358–1365, 2019.

[47] D. Britt, D. Tranchemontagne, and O. M. Yaghi, "Metal-organic frameworks with high capacity and selectivity for harmful gases," vol. 199, 2008.

[48] Y. Mathieu, M. Soulard, J. Patarin, and M. Molière, "Mesoporous materials for the removal

of SO 2 from gas streams," *Fuel Process. Technol.*, vol. 99, pp. 35–42, 2012.

[49] D. H. McCrea, A. J. Forney, and J. G. Myers, "Recovery of sulfur from flue gases using a copper oxide absorbent," *J. Air Pollut. Control Assoc.*, vol. 20, no. 12, pp. 819–824, 1970.

[50] S. Yin, S. G. He, and M. F. Ge, "Reaction between sulfur dioxide and iron oxide cationic clusters," *Chinese Sci. Bull.*, vol. 54, no. 21, pp. 4017–4020, 2009.

[51] H. Wu *et al.*, "Sulfur Dioxide Capture by Heterogeneous Oxidation on Hydroxylated Manganese Dioxide," *Environ. Sci. Technol.*, vol. 50, no. 11, pp. 5809–5816, 2016.

[52] K. Silas, W. A. W. A. K. Ghani, T. S. Y. Choong, and U. Rashid, "Carbonaceous materials modified catalysts for simultaneous SO2/NOx removal from flue gas: A review," *Catal. Rev. - Sci. Eng.*, vol. 61, no. 1, pp. 134–161, 2019.

[53] H. Zhang, W. Cen, J. Liu, J. Guo, H. Yin, and P. Ning, "Adsorption and oxidation of SO 2 by graphene oxides: A van der Waals density functional theory study," *Appl. Surf. Sci.*, vol. 324, pp. 61–67, 2015.

[54] U. Narkiewicz, A. Pietrasz, I. Pe, and W. Arabczyk, "Removal of SO 2 from gases on carbon materials," pp. 41–45, 2012.

[55] D. J. Babu *et al.*, "Adsorption of pure SO2 on nanoscaled graphene oxide," *RSC Adv.*, vol. 6, no. 43, pp. 36834–36839, 2016.

[56] B. Li and C. Ma, "Study on the mechanism of SO2 removal by activated carbon," *Energy Procedia*, vol. 153, pp. 471–477, 2018.

[57] C. S. De Lecea, "Factors controling the SO 2 removal by porous carbons : relevance of the SO 2 oxidation step," vol. 38, pp. 335–344, 2000.

[58] U. Narkiewicz, A. Pietrasz, I. Pe, and W. Arabczyk, "Removal of SO 2 from gases on carbon materials," p. 10026, 2012.

[59] E. Atanes, A. Nieto-Márquez, A. Cambra, M. C. Ruiz-Pérez, and F. Fernández-Martínez, "Adsorption of SO2 onto waste cork powder-derived activated carbons," *Chem. Eng. J.*, vol. 211–212, pp. 60–67, 2012.

[60] V. Gaur, R. Asthana, and N. Verma, "Removal of SO 2 by activated carbon fibers in the presence of O 2 and H 2 O," vol. 44, pp. 46–60, 2006.

[61] F. Sun, J. Gao, Y. Zhu, and Y. Qin, "Mechanism of SO2 adsorption and desorption on commercial activated coke," *Korean J. Chem. Eng.*, vol. 28, no. 11, pp. 2218–2225, 2011.

[62] H. Tseng, M. Wey, Y. Liang, and K. Chen, "Catalytic removal of SO2, NO and HCl from incineration flue gas over activated carbon-supported metal oxides," vol. 41, pp. 1079–1085, 2003.

[63] U. Burghaus, "Gas-surface interactions on two-dimensional crystals," *Surf. Sci. Rep.*, vol. 74, no. 2, pp. 141–177, 2019.

[64] A. Shokuhi Rad, M. Esfahanian, S. Maleki, and G. Gharati, "Application of carbon nanostructures toward so 2 and so 3 adsorption: A comparison between pristine graphene

and N-doped graphene by DFT calculations," *J. Sulfur Chem.*, vol. 37, no. 2, pp. 176–188, 2016.

[65] E. Salih *et al.*, "Theoretical study on simultaneous removal of SO2, NO, and Hg0 over graphene: competitive adsorption and adsorption type change," *J. Phys. Chem. C*, vol. 25, no. 2, pp. 141–177, 2019.

[66] N. Askari Ardehjani and D. Farmanzadeh, "DFT investigation of metal doped graphene capacity for adsorbing of ozone, nitrogen dioxide and sulfur dioxide molecules," *Adsorption*, vol. 25, no. 4, pp. 661–667, 2019.

[67] M. D. Esrafili, P. Mousavian, and F. Arjomandi Rad, "Adsorption of formamide over pristine and Al-doped boron nitride nanosheets: A dispersion-corrected DFT study," *J. Mol. Graph. Model.*, vol. 82, pp. 101–107, 2018.

[68] A. M. Dimiev, L. B. Alemany, and J. M. Tour, "Graphene oxide. Origin of acidity, its instability in water, and a new dynamic structural model," *ACS Nano*, vol. 7, no. 1, pp. 576–588, 2013.

[69] Cheaptubes.com, "Graphene Oxide What is Graphene Oxide?," 2016. [Online]. Available: https://www.cheaptubes.com/product-category/graphene-oxide/.

[70] W. S. Hummers and R. E. Offeman, "Preparation of Graphitic Oxide," *J. Am. Chem. Soc.*, vol. 80, no. 6, p. 1339, 1958.

[71] P. B. Arthi G and L. BD, "A Simple Approach to Stepwise Synthesis of Graphene Oxide Nanomaterial," *J. Nanomed. Nanotechnol.*, vol. 06, no. 01, pp. 2–5, 2015.

[72] Y. L. Zhong, Z. Tian, G. P. Simon, and D. Li, "Scalable production of graphene via wet chemistry: Progress and challenges," *Mater. Today*, vol. 18, no. 2, pp. 73–78, 2015.

[73] D. C. Marcano *et al.*, "Improved synthesis of graphene oxide," *ACS Nano*, vol. 4, no. 8, pp. 4806–4814, 2010.

[74] L. Liu, H. Gao, and J. Zhao, "Lizhao Liu, Haili Gao, and Jijun Zhao."

[75] L. Liu, J. Zhang, H. Gao, L. Wang, X. Jiang, and J. Zhao, "Tailoring physical properties of graphene : Effects of hydrogenation, oxidation, and grain boundaries by atomistic simulations," *Comput. Mater. Sci.*, 2015.

[76] V. Lee, "Electronic Structure Studies of Graphene and Graphene Oxide Interfaces," *ProQuest Diss. Theses*, p. 150, 2013.

[77] D. Kour, S. Sasan, and K. K. Kapoor, "Graphene oxide: an efficient carbocatalyst for the solvent-free synthesis of 2-(substituted benzoyl)-3-(substituted phenyl)imidazo[1,2-a]pyridines," *Journal of Chemical Sciences*, vol. 132, no. 1, Springer India, 2020.

[78] B. F. MacHado and P. Serp, "Graphene-based materials for catalysis," *Catal. Sci. Technol.*, vol. 2, no. 1, pp. 54–75, 2012.

[79] N. Yousefi, X. Lu, M. Elimelech, and N. Tufenkji, "Environmental performance of graphene-based 3D macrostructures," *Nat. Nanotechnol.*, vol. 14, no. 2, pp. 107–119, 2019.

[80] S. Yun, H. Lee, W. E. Lee, and H. S. Park, "Multiscale textured, ultralight graphene monoliths for enhanced CO2 and SO2 adsorption capacity," *Fuel*, vol. 174, pp. 36–42, 2016.

[81] S. T. Yang *et al.*, "Folding/aggregation of graphene oxide and its application in Cu2+ removal," *J. Colloid Interface Sci.*, vol. 351, no. 1, pp. 122–127, 2010.

[82] X. Yang, C. Chen, J. Li, G. Zhao, X. Ren, and X. Wang, "Graphene oxide-iron oxide and reduced graphene oxide-iron oxide hybrid materials for the removal of organic and inorganic pollutants," *RSC Adv.*, vol. 2, no. 23, pp. 8821–8826, 2012.

[83] W. Cen, M. Hou, J. Liu, S. Yuan, Y. Liu, and Y. Chu, "Oxidation of SO2 and NO by epoxy groups on graphene oxides: The role of the hydroxyl group," *RSC Adv.*, vol. 5, no. 29, pp. 22802–22810, 2015.

[84] D. H. Lan, F. M. Yang, S. L. Luo, C. T. Au, and S. F. Yin, "Water-tolerant graphene oxide as a high-efficiency catalyst for the synthesis of propylene carbonate from propylene oxide and carbon dioxide," *Carbon N. Y.*, vol. 73, pp. 351–360, 2014.

[85] Y. Long, C. Zhang, X. Wang, J. Gao, W. Wang, and Y. Liu, "Oxidation of SO2 to SO3 catalyzed by graphene oxide foams," *J. Mater. Chem.*, vol. 21, no. 36, pp. 13934–13941, 2011.

[86] F. He *et al.*, "Synthesis of three-dimensional reduced graphene oxide layer supported cobalt nanocrystals and their high catalytic activity in F-T CO2 hydrogenation," *Nanoscale*, vol. 5, no. 18, pp. 8507–8516, 2013.

[87] E. Humeres *et al.*, "Selective insertion of sulfur dioxide reduction intermediates on graphene oxide," *Langmuir*, vol. 30, no. 15, pp. 4301–4309, 2014.

[88] G. Zhao, J. Li, X. Ren, C. Chen, and X. Wang, "Few-layered graphene oxide nanosheets as superior sorbents for heavy metal ion pollution management," *Environ. Sci. Technol.*, vol. 45, no. 24, pp. 10454–10462, 2011.

[89] J. Li, D. Kuang, Y. Feng, M. Liu, F. Zhang, and P. Deng, "An enhanced electrochemical sensing platform integrated with graphene oxide and iron hydroxide colloid for sensitive determination of phloroglucinol," *J. Braz. Chem. Soc.*, vol. 24, no. 4, pp. 621–630, 2013.

[90] R. Nie *et al.*, "MnO 2/graphene oxide: A highly active catalyst for amide synthesis from alcohols and ammonia in aqueous media," *J. Mater. Chem.*, vol. 22, no. 35, pp. 18115–18118, 2012.

[91] M. Hegde *et al.*, "Strong graphene oxide nanocomposites from aqueous hybrid liquid crystals," *Nat. Commun.*, vol. 11, no. 1, pp. 1–7, 2020.

[92] M. E. Shabestari, O. Martín, D. Díaz-García, S. Gómez-Ruiz, V. J. Gonzalez, and J. Baselga, "Facile and rapid decoration of graphene oxide with copper double salt, oxides and metallic copper as catalysts in oxidation and coupling reactions," *Carbon N. Y.*, vol. 161, pp. 7–16, 2020.

[93] K. Zhang *et al.*, "Facile synthesis of monodispersed Pd nanocatalysts decorated on graphene oxide for reduction of nitroaromatics in aqueous solution," *Res. Chem. Intermed.*, vol. 45,

no. 2, pp. 599–611, Feb. 2019.

[94] I. Chemistry, “Graphene oxide and its application as adsorbent to wastewater treatment George Z. Kyzas, Eleni A. Deliyanni * and Kostas A. Matis.”

[95] M. B. Andrade, T. R. T. Santos, M. Fernandes Silva, M. F. Vieira, R. Bergamasco, and S. Hamoudi, “Graphene oxide impregnated with iron oxide nanoparticles for the removal of atrazine from the aqueous medium,” *Separation Science and Technology (Philadelphia)*, Taylor and Francis Inc., 02-Nov-2018.

[96] S. Presolski and M. Pumera, “Graphene Oxide: Carbocatalyst or Reagent?,” *Angew. Chemie - Int. Ed.*, vol. 57, no. 51, pp. 16713–16715, 2018.

[97] H. J. Song, X. H. Jia, N. Li, X. F. Yang, and H. Tang, “Synthesis of α-Fe 2O 3 nanorod/graphene oxide composites and their tribological properties,” *J. Mater. Chem.*, vol. 22, no. 3, pp. 895–902, Jan. 2012.

[98] C. Panaritis, J. Zgheib, S. A. H. Ebrahim, M. Couillard, and E. A. Baranova, “Electrochemical in-situ activation of Fe-oxide nanowires for the reverse water gas shift reaction,” *Appl. Catal. B Environ.*, vol. 269, no. October 2019, p. 118826, 2020.

[99] D. J. Babu *et al.*, “Adsorption of pure SO2on nanoscaled graphene oxide,” *RSC Adv.*, vol. 6, no. 43, pp. 36834–36839, 2016.

[100] C. Y. Cao, J. Qu, W. S. Yan, J. F. Zhu, Z. Y. Wu, and W. G. Song, “Low-cost synthesis of flowerlike α-Fe 2O 3 nanostructures for heavy metal ion removal: Adsorption property and mechanism,” *Langmuir*, vol. 28, no. 9, pp. 4573–4579, 2012.

[101] C. Li, Y. Shi, X. Chen, D. He, L. Shen, and N. Bao, “Controlled synthesis of graphite oxide: Formation process, oxidation kinetics, and optimized conditions,” *Chem. Eng. Sci.*, vol. 176, pp. 319–328, 2018.

[102] D. Titus, E. James Jebaseelan Samuel, and S. M. Roopan, *Nanoparticle characterization techniques*. Elsevier Inc., 2019.

[103] S. K. Kulkarni, *Nanotechnology: Principles and Practices*. 2015.

APPENDIX A

CALCULATIONS AND CHARACTERIZATION TECHNIQUES

A.1 Capture Capacity Calculations

The SO_2 capture capacity was calculated using the following formula: -

$$q = \frac{\left[\left(\int C_i - C_O\right)dT \times volumetric\ flowrate\right]}{Mass\ of\ material} \quad [A.1]$$

The $\left(\int C_i - C_O\right)dT$ term was calculated by subtracting the area under the curve of the sample (GO and GO-FexOy-P) of the area under the curve of the blank curves and the calculation sequence was followed:

$$Blank - Sample = Amount\ Adsorbed = a\ ppm.min \quad [A.2]$$

The area under the curve was calculated with the help of area under the curve using Trapezoidal rule using recorded concentration with time from the SO_2 detector:

$$area\ under\ the\ curve = \sum_{t=0}^{t=(t-1)} \{0.5 \times (y_2 + y_1) \times (x_2 - x_1)\} \quad [A.3]$$

Multiplying the amount adsorbed with the flow rate during the reaction:

$$a\ ppm.min \times f\frac{mL}{min} = (a \times f)\ ppm.mL \quad [A.4]$$

Applying the unit conversion:

$$= (a \times f)\ ppm.mL \times 10^{-6}\frac{\frac{mol\ SO_2}{mol}}{ppm} \times \frac{mol}{22400\ mL} \times \frac{64\ g\ SO_2}{mol\ SO_2} \quad [A.5]$$

Dividing the above equation with the mass of sample taken m = 50 mg

$$= \frac{(a \times f) \times 10^{-6} \times 64g\ SO_2}{22400} \times \frac{1000mg}{g} \times \frac{1}{50\ mg\ sample} \times 100 \quad [A.6]$$

$$= [(a \times f) \times (5.714 \times 10^{-6})]\frac{mg}{100\ mg\ GO} \quad [A.7]$$

This is the final equation obtained. The values for the amount adsorbed and flowrate were substituted and plotted as shown in Figure 4-4.

A.2 Additional TEM and EDXS analysis curves

Figure A-1 shows the EDXS and TEM (inset) analysis of GO-Fe_xO_y-P and GO-Fe_xO_y-P-S at different spectrum points. Figure A-1a. depicts the TEM (inset) and EDXS of the light region on the surface of GO-Fe_xO_y-P. Comparison of Figure A-1 a. and Figure 4.2 b. shows that the deposition of Fe on the surface of GO is not the same throughout the surface. The EDXS result does not show the peak of Fe, hereby confirming the non-uniformity of the Fe deposition.

Figure A-1b. depicts the TEM (inset) and EDXS of another dark region on the surface of GO-Fe_xO_y(P)-S. On comparing FigureA-1 b. and Figure 4.7 b. the EDXS also shows the approximately same level of S in both spectrums. Thus, the S capture seems to be uniform over the surface of GO-Fe_xO_y-P.

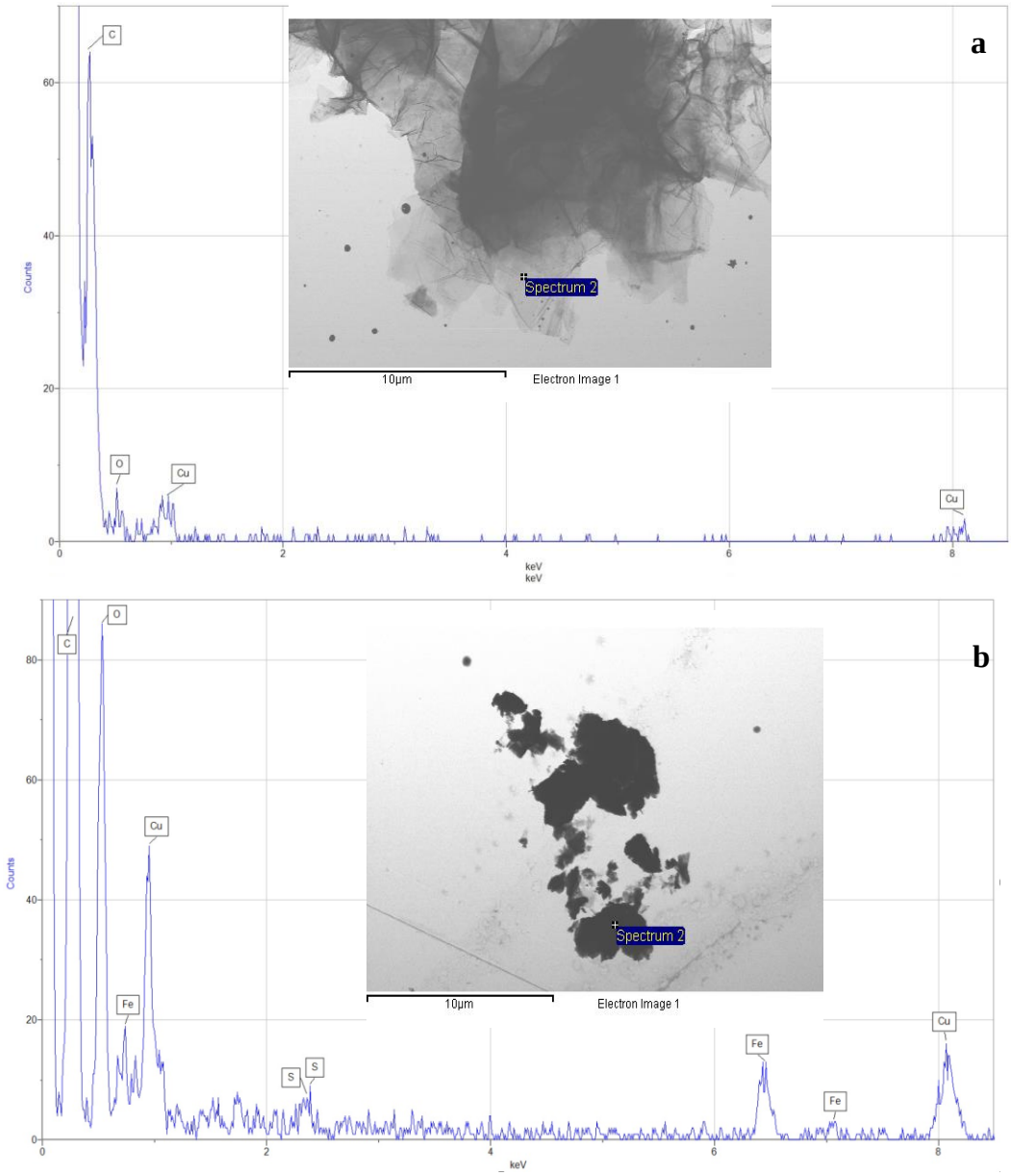

Figure A-1: EDXS and TEM images of a. GO-Fe_xO_y-P light spectrum, b. GO-Fe_xO_y-P-S dark area (2)

A.3 Characterization technique background

A.3.1 SEM

Scanning Electron Microscopy (SEM), helps us to observe the material on the micron level. The electron beam is directed towards the specimen from an electron gun located at the top of the device (see Figure 6-2). When the incident beam of electrons hits the surface of the specimen, X-rays and three types of electrons are emitted: backscattered (or primary) electrons, secondary electrons, and Auger electrons.

The SEM uses backscattered or primary and secondary electrons to cast high-resolution images. These images reveal details of around 1-5 nm using the secondary electrons.

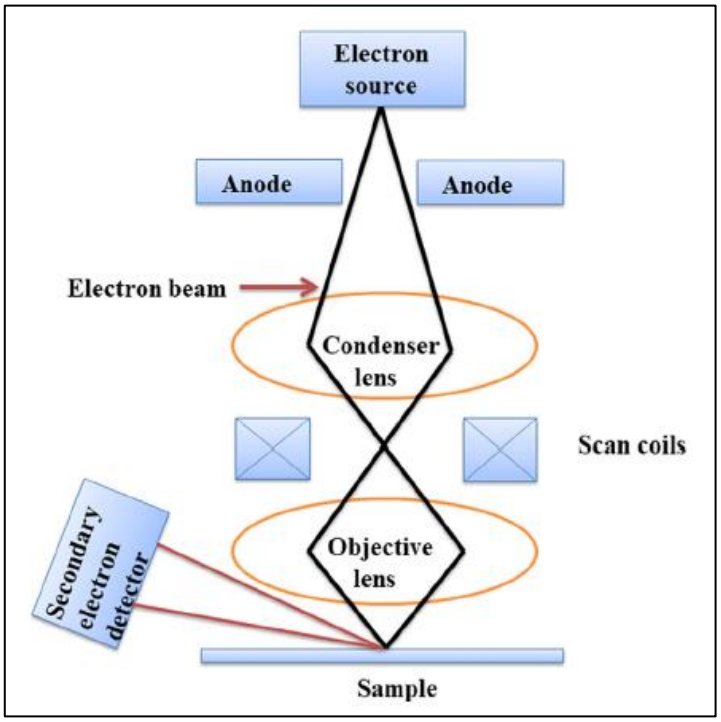

Figure A-2: Schematic of working SEM [102].

A.3.2 TEM

When the electron beam is transmitted through the sample, the interaction of the sample and the beam produces transmitted electrons through diffraction. The intensity of diffraction varies with respect to the plane of orientation. The electron beam, depending on the angles, is diffracted from certain points, and transmitted from others (see Figure 6-3).

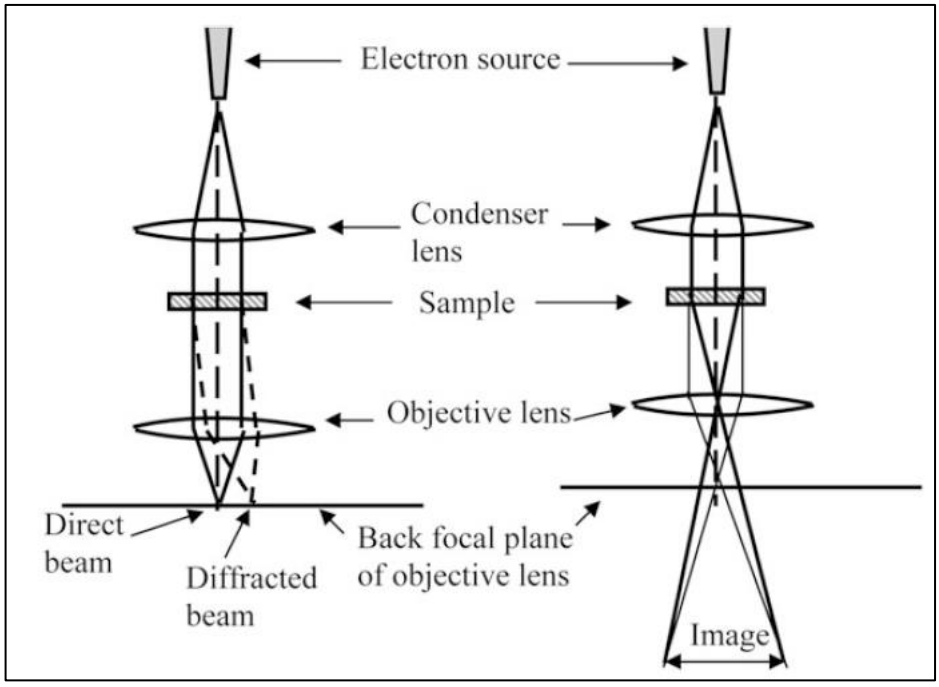

Figure A-3: Basic components of TEM [103].

A.3.3 EDXS

This technique gives an overall mapping of the sample by analyzing near-surface elements and estimates the elemental proportion at different positions.

The EDX is used in conjunction with SEM. The electron beam of energy of 10-20keV strikes the sample, causing X-rays to emit from the sample. The energy of the emitted X-ray depends on the sample. The X-rays generated are in the region of around 2 microns deep, thus it provides only the surface composition. By moving the electron beam source around the sample and with different angles, the images of the sample along with the composition at different spots can be obtained.

